Effect of cross-linking agents on the adsorption of histamine on molecularly imprinted polyacrylamide

Merymene Boukadida, Najeh Jaoued-Grayaa, Amira Anene, Yves Chevalier, Souhaira Hbaieb

Effect of cross-linking agents on the adsorption of histamine on molecularly imprinted polyacrylamide

Merymene Boukadida[a,b], Najeh Jaoued-Grayaa[c], Amira Anene[c], Yves Chevalier[a*], Souhaira Hbaieb[b*]

[a] Laboratoire d'Automatique, de Génie des Procédés et de Génie Pharmaceutique, Université de Lyon 1, UMR 5007 CNRS, 69622 Villeurbanne Cedex, France.
[b] Laboratoire de Recherche: Caractérisations, Applications et Modélisation de Matériaux, Université de Tunis El Manar, Faculté des Sciences de Tunis, Campus universitaire El Manar, Tunisia.
[c] Unité Spécialisée de développement des techniques analytiques, Institut National de Recherche et d'Analyse Physico-chimique, Biotechpole Sidi-Thabet, 2020 Ariana, Tunisia.

* Corresponding authors: Yves Chevalier: yves.chevalier@univ-lyon1.fr
Tel: +33 472 431 877
Souhaira Hbaieb: souhaira.hbaieb@fst.utm.tn
Tel: +216 98 94 74 79 Fax: +216 71 53 76 88

GRAPHICAL ABSTRACT

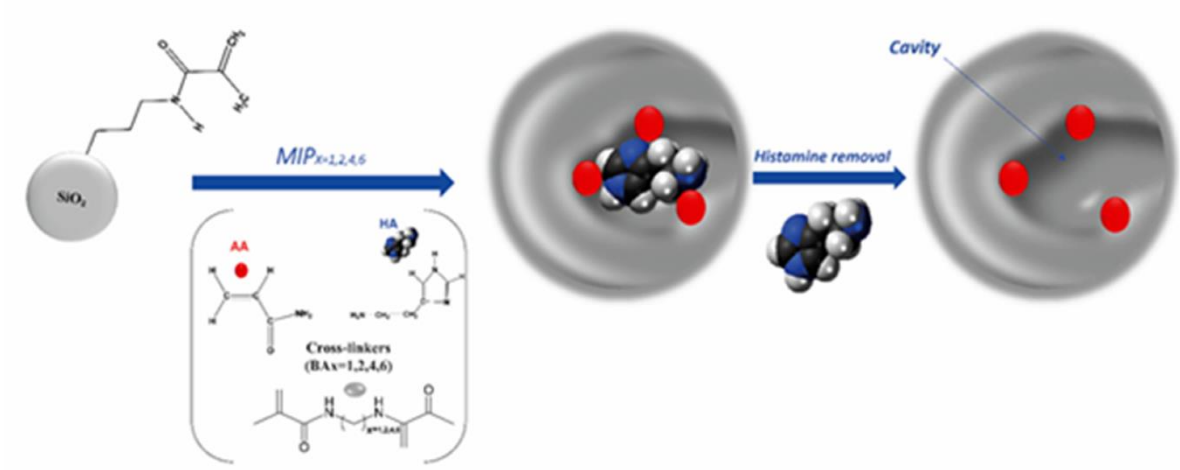

HIGHLIGHTS

- Flexible spacer of cross-linking agent improves the performance of MIPs.
- MIP as thin layers of cross-linked polyacrylamide selectively binds histamine.
- Selective and non-selective adsorption from modeling adsorption thermodynamics.

ABSTRACT

The ability of molecularly imprinted polymers (MIPs) prepared with flexible cross-linking agents for selective uptake of guest molecules is investigated. New polyacrylamide polymers had been synthesized for histamine (HA) extraction using solid supports based on MIPs immobilized on silica surface (SiO_2). The MIPs were prepared via radical polymerization in acetonitrile and in the presence of azobisisobutyronitrile (AIBN) as initiator, using HA as a target molecule, acrylamide as a functional monomer and several cross-linking agents having alkyl spacers of various lengths: *N*,*N*'-methylenebisacrylamide (BA_1), *N*,*N*'-ethylenebisacrylamide (BA_2), *N*,*N*'-(butane-1,4-diyl)-bis(2-methacrylamide) (BA_4) and *N*,*N*'-(hexane-1,6-diyl)-bis(2-methacrylamide) (BA_6). All the prepared MIPs have a strong absorption capacity of HA compared to non-imprinted polyacrylamide (NIPs). MIP_4 made with the BA_4 cross-linker shows a higher selectivity for adsorption of HA than MIPs made with BA_1, BA_2 and BA_6. Thus, the imprinting factor for adsorption from a 5 ppm HA solution was 2.5 for MIP_4 against 1.4 to 1.6 for MIP_1, MIP_2 and MIP_6. Langmuir–Volmer and Volmer models of the adsorption isotherms of MIPs and NIPs accurately fit the experimental data. They provide the characteristic parameters of the adsorption thermodynamic of the materials. The higher performance of MIP_4 for selective adsorption of HA is mainly coming from a higher density of molecular imprints (1.4 $\mu mol \cdot m^{-2}$ against 0.13–0.15 $\mu mol \cdot m^{-2}$ for MIP_1 and MIP_2 and 0.4 $\mu mol \cdot m^{-2}$ for MIP_6) than a higher affinity of HA for the molecular imprints. The selectivity with respect to the tyramine and melamine interfering molecules is also higher for MIP_4. As the main outcome, some moderate flexibility of the material is advantageous. Such flexibility allows for a reversible healing and re-opening of the molecular imprints as the HA guest is removed and back-adsorbed.

Keywords. Molecularly imprinted polyacrylamide, Histamine, Cross-linking agent effects.

1. Introduction

Molecularly Imprinted Polymers (MIPs) are made of densely cross-linked polymer where the presence of a guest molecule during polymerization leaves a shape memory as a molecular imprint able to selective recognition of the guest molecule [1]. Such materials showing selective binding of the target guest molecule find many types of applications where a molecular recognition is wished: stationary phases of HPLC and preconcentration SPME cartridges, chemical sensors, catalysis… [2,3,4,5]. The conventional molecular imprinting technique involves extensive cross-linking yielding highly rigid structures [6]. Cross-linking the polymer materials increases their mechanical strength and stiffness [7]. In the framework of MIPs, the purpose of the dense cross-linking is freezing the shape of the guest molecule acting as a template during the polymerization process. A too large amount of cross-linker nevertheless seems detrimental to the selective adsorption properties. The choice of the cross-linker and the optimum cross-linking density depend on the specific case (type of target molecule and type of application) and which criterion is considered for the determination of the optimum. Thus, Sellergren stated that divinylbenzene (DVB) was not suitable because of "lower selectivity, poorer chromatographic performance" [8]. Conversely, DVB was preferred by Muhammad et al. because of a higher selectivity expressed by the imprinting factor (*IF*), but at the expense of the binding capacity [9]. The optimum monomer:cross-linker ratio was found for 1:1 in the case of the chromatographic separation of L-phenylalanine anilide using the classical (methacrylic acid-EGDMA)-based MIPs [10]. A similar ratio of 35:50 was used by da Mata et al. [11] in the case of glyphosate extraction by a polyacrylamide-based MIP. Much higher amounts of cross-linker were determined as optimum in more recent studies [12,13,14]. An opposite conclusion was reached, giving the optimum ratio of 12 mol%, based on measurements of the binding capacity (instead of selectivity) in a quite low and narrow range of such ratio [15]. An NMR investigation of polyacrylamide gels cross-linked with *N*,*N*'-methylene-bis-acrylamide (BA_1 in

the present study) showed that the onset of solid-like behavior of the gel was reached at 40 wt% cross-linker [16]. As an outcome, there is a large variety of case, all of them appearing specific, so that it is difficult to draw general trends from several reports of studies performed under various specific conditions. Owing to the many parameters of relevance, approaches by multivariate analysis allow reaching interesting conclusions [17,18]; they remain restricted to specific cases however. Selecting the appropriate cross-linker is critical for improving the recognition performance of imprinted polymers. A systematic study on the cross-linker under control of the other parameters is needed.

Acrylamide has been identified as a suitable functional monomer for the manufacture of MIPs because of its ability to bind many types of molecules by means of hydrogen bonds [19]. Acrylamide binds histamine (HA) as a model basic compound [20]. The acrylamide monomer and polyacrylamide show strong hydrogen bonding interactions with HA. Considering their similar reactivity in free radical polymerization, alkylenebisacrylamides appear well-suited as cross-linking agents of polyacrylamide for providing the imprinted polyacrylamide a high degree of selectivity [16].

The choice of the cross-linker for optimum performance of the MIPs is addressed. Importantly, variations of the polymethylene spacer length of the cross-linker may control the flexibility around the molecular imprints that allows favorable structural rearrangements for rebinding the guest molecule. Four MIPs were studied utilizing four different types of *N*,*N*'-polymethylenebis(acrylamide) cross-linkers with spacers of 1 to 6 methylenes BA_1, BA_2, BA_4 and BA_6. The non-imprinted polymers (NIPs) were made under identical conditions as the imprinted polymers but without the HA. The adsorption performances of MIPs toward HA molecules were studied, as well as competitive adsorption with possible interfering substances.

2. Materials and Methods

2.1. Materials and reagents

Fumed silica was used, which is an amorphous pyrohydrolysis silica manufactured by Degussa under the brand name Aerosil 200. (3-Aminopropyl)triethoxysilane (APTES, 99%), methacryloyl chloride (97%), diisopropylethylamine (99%), triethylamine (99%), histamine (HA, 97%), tyramine (TYR, 98%), melamine (MEL, 99%), acrylamide (AA, ≥ 99%), *N*,*N*'-methylenebisacrylamide (BA_1, ≥ 99.5%), *N*,*N*'-ethylenebisacrylamide (BA_2, ≥ 99.5%), 1,4-diaminobutane (99%) and 1,6-diaminohexane (99%) for the synthesis of *N*,*N*'-(butane-1,4-diyl)-bis(2-methacrylamide) (BA_4) and *N*,*N*'-(hexane-1,6-diyl)-bis(2-methacrylamide) (BA_6), Na_2SO_4, azobis(isobutyronitrile) (AIBN, 98%), tetrahydrofuran (THF), acetonitrile, methanol (MeOH), ethanol (EtOH), dichloromethane, toluene, LC-MS grade ammonium acetate and formic acid were all purchased from Sigma-Aldrich. Water of resistivity > 18 MΩ·cm was delivered by a Millipore water purification system (Bedford, MA).

2.2. Materials synthesis

2.2.1. Modification of the silica surface

The silica has been dehydrated at 140 °C for 2 h before grafting the organosilane to its surface. SiO_2 was modified in two steps [21] (Figure 1): methacryloylamidopropyltriethoxysilane (APTESMA) was first synthesis by the reaction of APTES and methacryloyl chloride, and APTESMA was chemically grafted to silica in a second step.

Step I: To a solution of APTES (2.5 mL, 14.32 mmol) in 60 mL of toluene was added the triethylamine (3 mL, 22.22 mmol) and methacryloyl chloride (2.5 mL, 25.58 mmol) dissolved in 40 mL of toluene. The reaction mixture was left under stirring at room temperature for 48 h, then filtered. The filtrate was evaporated to dryness under reduced pressure and purified by chromatography on silica gel using (80/20 v/v: hexane/ethyl acetate) as eluent to give a yellowish oil product (APTESMA).

Step II: To 5 g of activated silica dispersed in 150 mL of toluene was added 5 mL of diisopropylethylamine, followed by 3 g (12.13 mmol) of APTESMA synthesized product diluted in 50 mL of toluene. During 24 h, the mixture was kept at a temperature of 120 °C while being stirred. When the reaction was completed, the content was filtered and washed with THF. The obtained modified silica SiO_2(APTESMA) material was dried in an oven at 60 °C and then stored for later uses.

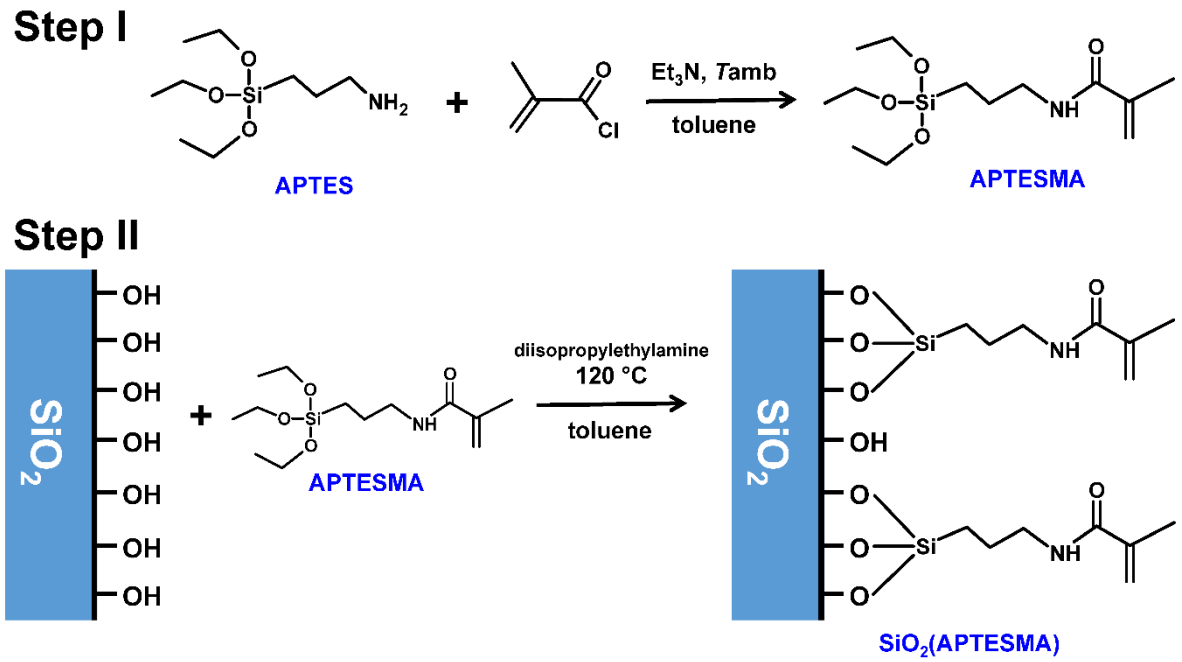

Figure 1. Reaction schemes for the preparation of the methacryloyl-modified silica SiO_2(APTESMA). *Step I:* Synthesis of APTESMA. *Step II:* Grafting of APTESMA onto the silica surface.

2.2.2. Preparation of histamine imprinted polyacrylamide polymers

Imprinted polyacrylamide polymers were synthesized using radical polymerization as follows: 1 mmol of HA dissolved in 20 mL of acetonitrile was added to 500 mg of modified silica SiO_2(APTESMA). The reaction mixture was stirred until the temperature reached 80 °C. Thereafter, 0.2 mmol of the initiator AIBN was added, followed by 8 mmol of AA and 8 mmol of the corresponding cross-linker (BA_1, BA_2, BA_4, BA_6). The reaction mixture was stirred for 24 h. Then, the obtained material was filtered and washed with THF. The four obtained solids

named as MIP_1, MIP_2, MIP_4, MIP_6 were dried in an oven, ground, and stored for later uses. To remove the template molecules, the prepared materials were extracted in a Soxhlet apparatus using methanol for 72 h [22]. Finally, the MIPs were thoroughly washed with deionized water for 72 h and dried in a vacuum oven for 24 h. Non-imprinted polymer materials NIP_1, NIP_2, NIP_4 and NIP_6 were prepared in the same experimental conditions as MIPs, but in the absence of HA molecule.

2.2.3. Synthesis of the cross-linking agents

The synthesis procedure of cross-linkers BA_4 and BA_6 [23,24] is summarized in Figure 2. To a solution of methacryloyl chloride (50 mmol, 5 mL) dissolved in dichloromethane (20 mL) was added dropwise a mixture of 1,4-diaminobutane (24 mmol, 2.41 mL) or 1,6-diaminohexane (24 mmol, 3.13 mL) and triethylamine (50 mmol, 6.75 mL) in water (50 mL) at temperature 0–5 °C. The mixture rapidly turned heterogeneous upon the addition because water and dichloromethane are not miscible. After 2 h, the mixture was extracted with dichloromethane (3×10 mL). The combined organic phases were dried over Na_2SO_4, filtered and concentrated under reduced pressure. The crude product was then purified by precipitation in hexane to afford monomer (BA_4 or BA_6) as a white solid powder. ^1H and ^{13}C NMR, IR and MS analyses are as follows:

- *N,N*'-(butane-1,4-diyl)-bis(2-methacrylamide) (BA_4)

Yield: 74 %. ^1H NMR (500.13 MHz, DMSO-d_6) δ (ppm): 7.93 (s, 2H); 5.63 (s, 2H); 5.31 (s, 2H); 3.11 (s, 6H); 1.84 (s, 4H); 1.42 (s, 4H). ^{13}C NMR (125.76 MHz, DMSO-d_6) δ (ppm): 167.8 (2); 140.6 (2); 119.1 (2); 39.1 (2); 27.1 (2); 19.1 (2).

IR (ATR, ν (cm^{-1}): 3312 (N–H); 2925 and 2860 (sym C–H and asym C–H); 1651 (C=O); 1530 (C=C); 1173 (C–N).

HRMS ESI^+ *m/z*: calculated for $C_{12}H_{20}N_2O_2H^+$: 225 .1598; found: MH^+: 225.1598.

- *N,N*'-(hexane-1,6-diyl)-bis (2-methacrylamide) (BA_6)

Yield: 83 %. ^{1}H NMR (500.13 MHz, DMSO-d_6) δ (ppm): 7.89 (s, 2H); 5.62 (s, 2H); 5.29 (s, 2H); 3.11 (s, 6H); 1.84 (s, 4H); 1.42 (s, 4H); 1.25 (s, 4H). ^{13}C NMR (125.76 MHz, DMSO-d_6) δ (ppm): 167.8 (2); 140.6 (2); 119.1 (2); 39.2 (2); 29.5 (2); 26.6 (2); 19.1 (2).

IR (ATR, ν (cm^{-1}): 3324 (N–H); 2928 and 2854 (sym C–H and asym C–H); 1655 (C=O); 1531 (C=C); 1176 (C–N).

HRMS ESI^{+} *m*/*z*: calculated for $C_{14}H_{24}N_2O_2H^{+}$: 253.1911; found: MH^{+}: 253.1911.

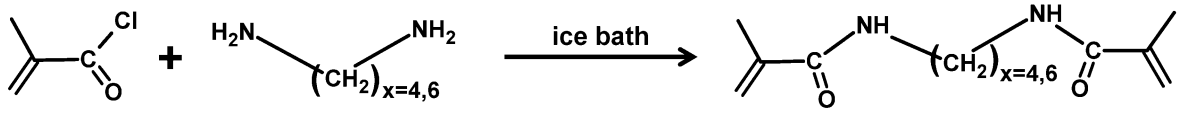

Figure 2. Synthesis of the cross-linkers BA_4 and BA_6.

2.3. Methods

Thermogravimetric analysis (TGA) measurements were carried out using a TG 209 F1 Netzsch instrument in the temperature range of 25–1000 °C at a heating rate of 10 °C·min^{-1} in a nitrogen gas flow. A Perkin-Elmer 2400 series II equipment was used for C H N analysis. The infrared spectra were carried out in the wavenumber range 400–4000 cm^{-1} using a Bruker IFS 55 Equinox FTIR spectrometer in ATR mode. A Bruker Avance III 500.13 ultra shield Plus spectrometer was used to obtain ^{1}H NMR as well as ^{13}C and solid-state ^{13}C and ^{29}Si NMR spectra at 500.13 MHz, 125.76 MHz and 59.62 MHz, respectively. The specific surface areas were measured by BET experiments at 77 K using a Micromeritics ASAP2020 instrument. The MIP and NIP samples were heated at 150 °C under vacuum before nitrogen adsorption measurements. The full nitrogen adsorption-desorption isotherms were collected and the Brunauer-Emmett-Teller (BET) equation was used to calculate the specific surface area. Images of transmission electron microscopy (TEM) were obtained using a Philips CM120 microscope set at 80 kV acceleration voltage. A drop of a dispersion of the materials in water was deposited on a formvar copper grid and dried before observation by TEM. Zeta potential measurements

of aqueous suspensions of the materials were performed by electrophoresis in DTS1070 U-shaped cells using a Malvern NanoZS instrument (Malvern, UK). The calculation of the zeta potential from the electrophoretic mobility was done using the Henry equation under the Smoluchowki approximation. Chromatography measurements were carried out using the Agilent 1290 Infinity LC system coupled to the Agilent 6490 Triple Quadrupole LC/MS System with Agilent Jet Stream Technology. Chromatographic separation of histamine was carried-out on Waters XBridge® BEH C18 2.5 µm 3.0×150 mm XP Column at 25 ± 1 °C with an isocratic flow rate of 0.30 mL·min^{-1} and the injection volume was 10 µL·min^{-1} and the UV detector was set at 254 nm. The mobile phases were 10 mM ammonium acetate in water containing 0.1 % formic acid (mobile phase A) and acetonitrile (mobile phase B) in a 65/35 v/v ratio. The autosampler was kept at a constant temperature of 20 ± 1 °C. The electrospray MS detector was used in a positive mode (ESI^+) to ionize neutral histamine molecules to molecular ions. The desolvation gas (nitrogen) was heated to 350 °C, whereas the ion source was at 120 °C. The capillary and cone voltages were 4 kV and 10 V, respectively. The collision gas was argon, and the collision energy was set to 10 V. The mass spectrometer was set to MRM (multiple reaction monitoring) modes, and the molecular ion used for quantification of HA was m/z = 112 g·mol^{-1} [25]. For the selectivity study, the molecular ions for the quantification of TYR and MEL were respectively m/z = 138 g·mol^{-1} and 127 g·mol^{-1}.

2.4. Binding experiments

Equilibrium adsorption experiments were carried out by mixing 30 mg of MIP or NIP with 5 mL of deionized water at different initial concentrations of HA (45–2700 µmol·L^{-1}). After a 20 min equilibration time, the mixture was centrifuged at 10000 rpm, the molecular ion m/z 112 g·mol^{-1} corresponding to HA was used to calculate the residual concentration of HA in the supernatant using LC-MS as a detection method. For kinetics experiments, the same method

was used but for various contact times (5–40 min). The calibration curves and the chromatogram of HA are given in section S.5 of Supporting Information.

Eq. 1 was used to calculate the adsorbed amount at time *t*:

$$Q(t) = \frac{(C(0)-C(t))V}{m\,A_{SP}} \quad (1)$$

where $Q(t)$ (mol·m^{-2}) is the adsorption capacity at time *t*; $C(0)$ (mol·L^{-1}) and $C(t)$ (mol·L^{-1}) are the concentrations of HA at initial and time *t*; *V* (L) is the volume of HA solution, *m* (g) is the mass of adsorbent, and A_{SP} is the specific surface area (m^2·g^{-1}).

The imprinting efficiency of the imprinted material was defined as follows:

$$IF = \frac{Q_e(\mathrm{MIP})}{Q_e(\mathrm{NIP})} \quad (2)$$

where Q_e(MIP) (mol·m^{-2}) and Qe(NIP) (mol·m^{-2}) are the adsorbed quantities of HA at equilibrium for the MIP and NIP [26].

2.5. Selectivity study

Adsorption of HA and structurally similar chemicals TYR and MEL was measured from 5 mL of this mixed solution at 45 µmol·L^{-1} in deionized water at pH 5.5 to 30 mg of MIP_4 or NIP_4 materials. At the equilibrium time (40 min), the amount of analyte adsorbed by MIP_4 or NIP_4 was determined using equation (1). The selectivity for HA with regards to competitive species (TYR and MEL) acting as interfering molecules was characterized by the distribution coefficient (*D*, L·g^{-1}) and the selectivity factor (α) calculated using Eqs 3 and 4 [27]:

$$D = \frac{Qe}{Ce} \quad (3)$$

with Q_e (mol·m^{-2}) being the adsorbed amount and C_e (mol·L^{-1}) being the concentration remaining in solution at equilibrium;

$$\alpha = \frac{D\mathrm{analyte,MIP}}{D\mathrm{competitor,MIP}} \quad (4)$$

3. Results and Discussion

3.1. Synthesis and characterization of MIPs and NIPs materials

A combination of the surface imprinting method and the use of a stiff polyacrylamide polymer was investigated to prepare HA imprinted polymers. The modification of SiO_2 using APTES coupled to methacryloyl chloride is essentially based on a direct reaction between the SiO_2 surface containing silanol groups and reactive groups of the organosilane to yield a solid support to be used in the synthesis of MIPs and NIPs. The reaction is carried out in anhydrous medium on a dry substrate, preventing the hydrolysis of the silane. The grafting density of APTESMA onto SiO_2 was 6.21 $\mu mol \cdot m^{-2}$ according to thermogravimetric analyzes, and 6.44 $\mu mol \cdot m^{-2}$ and 6.26 $\mu mol \cdot m^{-2}$ inferred from elemental analyses of carbon and nitrogen. The difference of grafting density obtained by elemental chemical analysis (EA) and thermogravimetric analyzes is due to incomplete condensation of methoxy groups [25]. All characterizations (IR, EA, ^{13}C CP-MAS NMR, ^{29}Si CP-MAS NMR) have been made for modified silica and all details are reported in section S.1 of Supporting Information confirming the successful grafting.

HA-imprinted polyacrylamide materials were synthesized using the four cross-linkers BA_1, BA_2, BA_4 and BA_6 differing by the length of their polymethylene spacer, and using AA as a functional monomer. The conventional free radical polymerization in solution was used with AIBN as initiator and acetonitrile as the solvent. The use of an aprotic solvent allows maintaining the stability of the formed pre-polymerization complex by favoring the interaction between the template and the functional monomers as avoiding the too strong interactions with the solvent molecules. NIPs were prepared under the same polymerization conditions except that the HA guest molecule was absent in the polymerization process.

The IR spectra of all the synthesized polymers were identical [28]. The IR spectrum of NIP showed peaks that were similar to those of MIP, indicating that HA was well extracted from the polymer matrix. The IR spectra of MIP_4 and NIP_4 materials (Figure 3) showed a broad

absorption band in the range 3500–3200 cm^{-1} associated with the O–H vibration of moisture and N–H stretching vibration of the secondary amide group. Secondary amides are revealed by stretching vibrations of C=O bonds and amide II band centered around 1605 cm^{-1} ($\nu_{C=O}$) and 1570–1510 cm^{-1} (δ_{N-H} and ν_{C-N}). The stretching vibrations of C–H bonds of CH_3 and CH_2 groups as a broad composite band in the 3100–2850 cm^{-1} range. Stretching vibrations of the silica Si–O–Si as well as the out-of-plane deformation of the CH_2 groups gave an absorption at 1100–1000 cm^{-1}. In the spectra of MIP_4 and NIP_4 compared to that of SiO_2(APTESMA), the absorbance of Si–O–Si relative to all other bands was less because polymerization increased the amounts of organic materials.

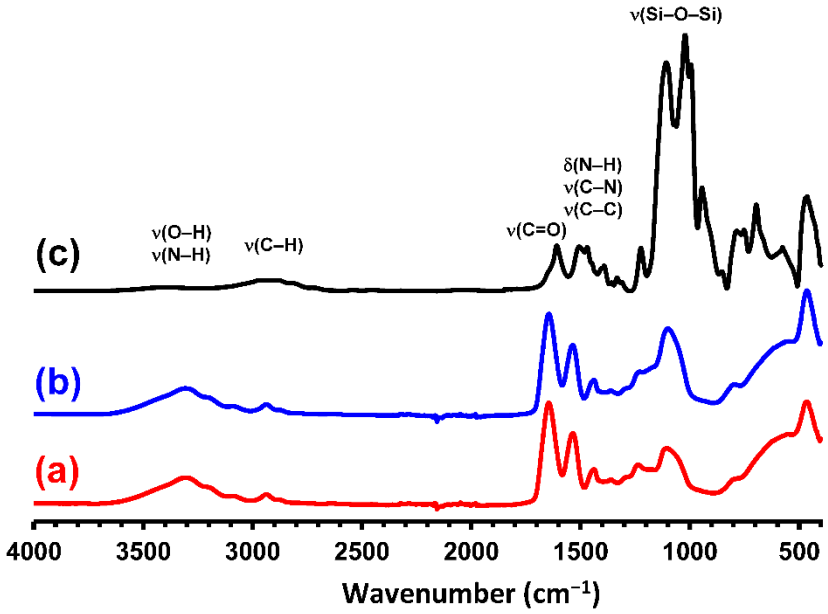

Figure 3. IR spectra of MIP_4 (a), NIP_4 (b), and SiO_2(APTESMA) modified silica (c).

The ^{13}C CP-MAS NMR spectra of MIP and NIP (Figure 4) revealed a characteristic peak of the C=O group of the amide function at 202.89 ppm, as well as other characteristic peaks of C=C at 123.44 and 162.37 ppm and those of C–C at 27.62 and 84.94 ppm, confirming the formation of the polymer layer on the surface of the modified silica. The similar spectra of imprinted and non-imprinted polymers showed that histamine extraction from the MIP was successful.

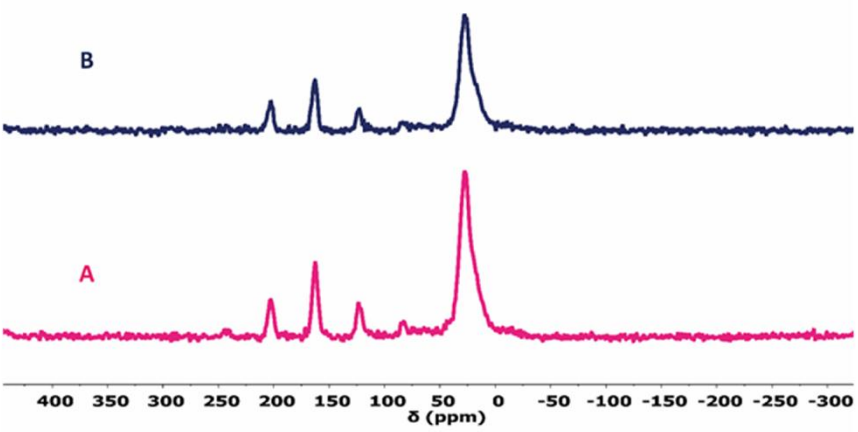

Figure 4. ^{13}C CP-MAS NMR spectra of MIP (A) and NIP (B).

Thermogravimetric analysis of the imprinted materials and the non-imprinted materials was used to infer the mass fraction of organic polymer in the MIPs and NIPs (Figure S5 in section S.2 of Supporting Information). The TGA curves of each MIP and NIP were identical, showing that the presence of the template molecules during the MIP polymerization did not affect the amount of polymer attached to the silica, and confirming that the histamine has been removed to completion during the washing step. The mass fraction of grafted polymer was taken as the mass loss between 200 and 500 °C in the TGA curves [29]. A slight but significant increase in the mass fraction of grafted polymer material was noted as going from MIP_1/NIP_1, to MIP_2/NIP_2, MIP_4/NIP_4, and finally MIP_6/NIP_6 (Table 1), which was explained by the increase in the polymethylene chain of the cross-linking agents of the various polymers materials.

Table 1. Mass losses of the different synthesized MIPs and NIPs.

Polymer	MIP_1	NIP_1	MIP_2	NIP_2	MIP_4	NIP_4	MIP_6	NIP_6
Mass loss (%)	53.5	51.9	61.5	58.3	80.2	79.5	86.9	85.1

BET measurements of nitrogen gas adsorption at 77 K were used to evaluate the specific surface area of the MIPs and NIPs. The adsorption-desorption isotherms of nitrogen gas (Figure S6) were similar: they were of the type II of the IUPAC classification [30]; and adsorption and

desorption profiles did not show significant hysteresis. The Harkins–Jura analysis did not reveal microporosity. The BET specific surface area determined by fitting the BET equation to the adsorption branch below 0.3 relative pressure were all of the order A_{SP} = 100 $m^2 \cdot g^{-1}$ (Table S2). The morphology of MIP and NIP synthesized materials has been characterized by means of transmission electron microscopy observations. TEM images of MIP and NIP at various magnifications (Figure 5) revealed that the particles were spherical and homogenous in shape with a narrow size distribution in the range of 20–100 nm. Image analysis of the TEM images gave the average particle size of 11.0 ± 0.7 nm with a standard deviation of 1.86 nm.

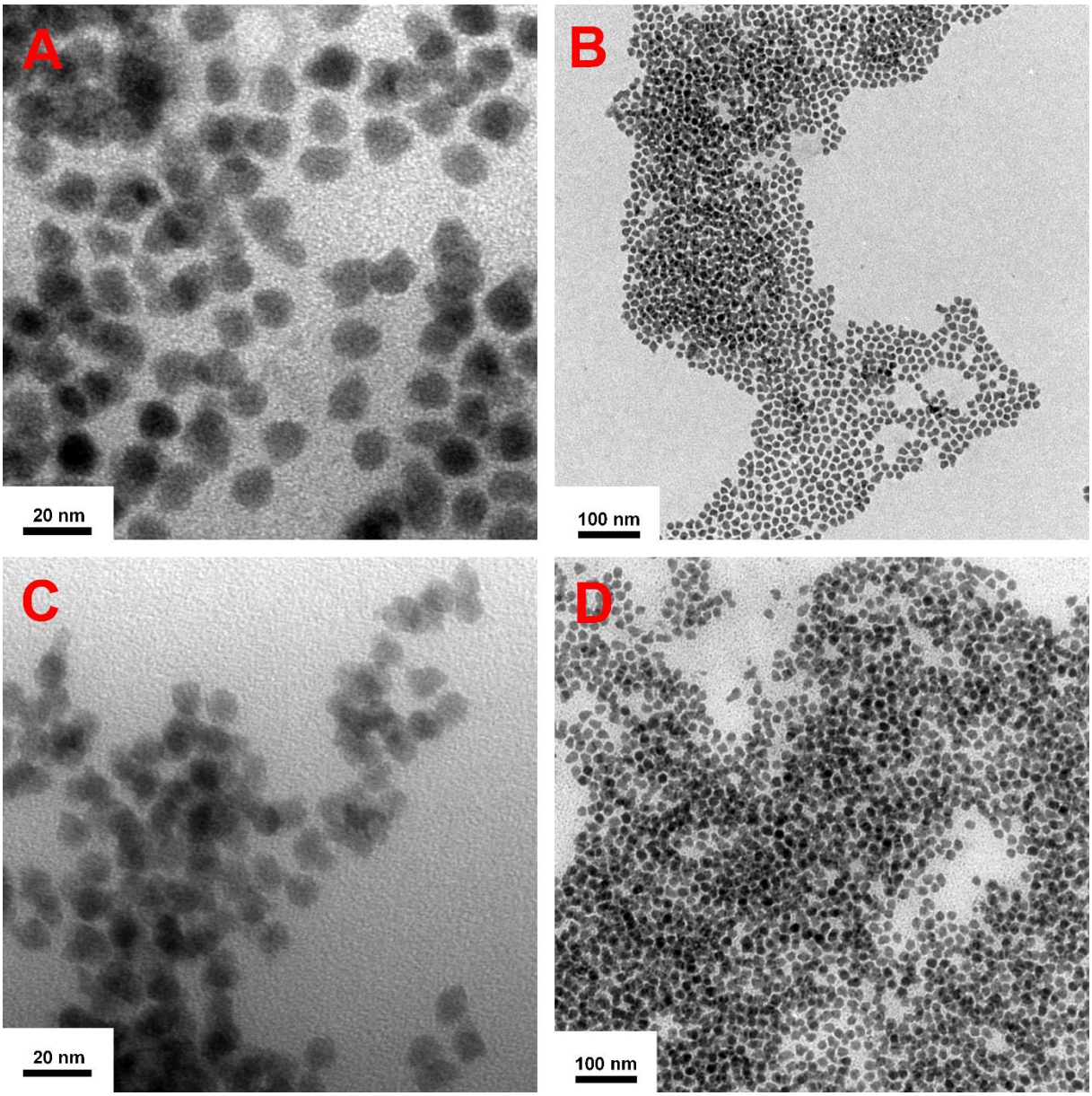

Figure 5. TEM images of MIP (A, B) and NIP (C, D) at two magnifications (scale bars are 20 nm and 100 nm).

The pH of the solution is an important parameter in the adsorption process. Indeed, the variation of pH directly affects the surface charge of the adsorbent and the molecular structures of the adsorbates, which makes it essential to study the effect of this factor on the retention capacity of HA. According to the potential zeta measurements of the MIP_4 and NIP_4 particles as a function of pH (Figure 6), the isoelectric point was at pH 4.7, which is significantly different from the isoelectric point of the modified silica at pH 2.0. The surface charges of MIP and NIP are positive for pH < 4.7 and negative for pH > 4.7.

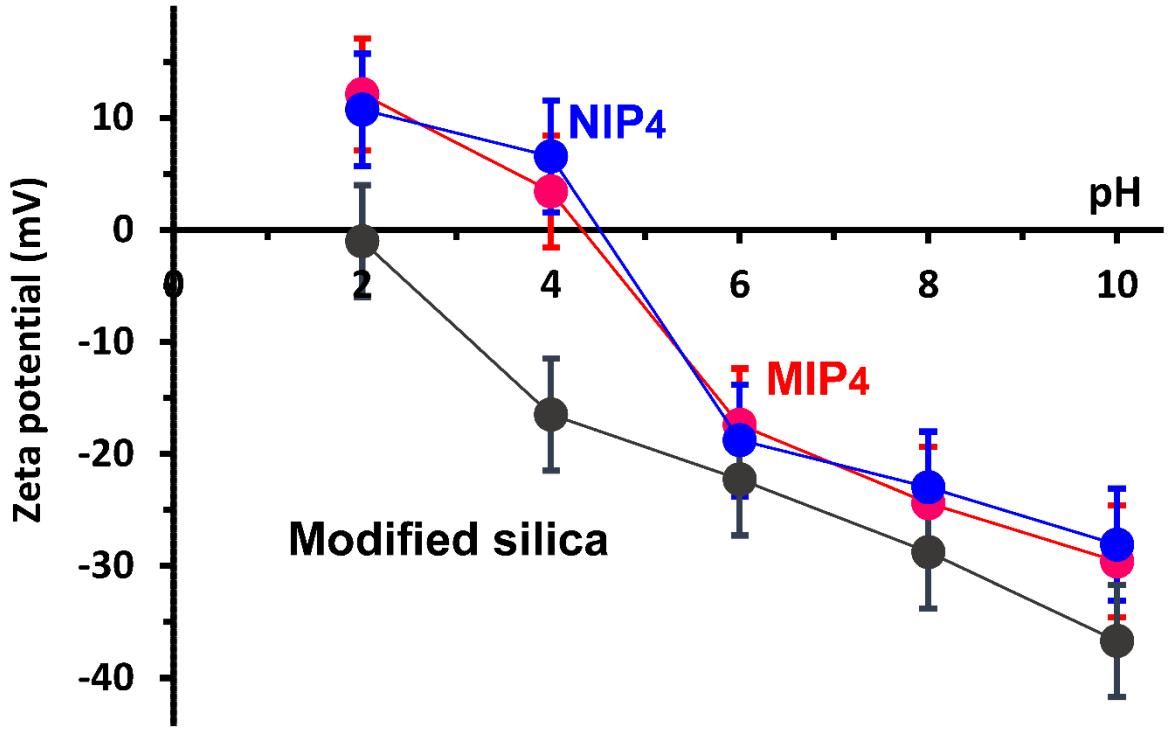

Figure 6. Zeta potential measurements of MIP and NIP as a function of pH.

3.2. Evaluation of the adsorption properties of MIPs and NIPs

3.2.1. Adsorption experiments

The thermodynamic equilibrium between adsorbed and free HA molecules is represented by "adsorption isotherms" that link their respective concentrations $Q(\mu mol \cdot m^{-2})$ and $C(mol \cdot L^{-1})$.

Bisacrylamides were specifically used as cross-linking agents for imprinting polyacrylamides with HA since they provide the polymer with high flexibility and conformational adaptability. pH is a key parameter impacting adsorption behavior; it strongly influences electrostatic interactions that affect the adsorbent and adsorbate properties. Due to the p*K*a values of HA (5.8, 9.4 and 14), the strong positive charge was shifted to negative by varying the pH from 5.5 to 11.4. Temperature changes allow us to evaluate the relative contributions of enthalpy and entropy to the free energy of adsorption. Finally, the adsorption kinetics was studied due to the importance of this parameter for the use of MIPs as chromatographic stationary phases.

Selective interactions are used to bind HA to molecular imprints, thus supplementing the non-selectivity of electrostatic interactions. Adsorption measurements to NIP were used to evaluate the contribution of non-selective interactions to the binding. The comparison of MIP and NIP adsorption behavior is obvious in MIP-related works. The "Imprinting Factor" (*IF*) is defined as the ratio of adsorptions of MIP and NIP that demonstrates selective adsorption to molecular imprints.

3.2.2. Thermodynamics of equilibrium adsorption

Equilibrium adsorption isotherms have been measured for adsorption of HA to all MIP and NIP materials after an equilibration time of 40 min. Their analysis using may be done with the help of various thermodynamic models. The Langmuir isotherm model is the most basic of them; it assumes that molecules are adsorbed on specified sites on the adsorbent surface and that MIPs have a single affinity constant value and homogeneous binding sites. Thus, the adsorption is localized, as opposed to the non-localized adsorption model of Volmer for which adsorbate molecules can move freely on the adsorbent surface. As a result, the Langmuir model was used for localized adsorption to the molecular imprints and the Volmer model was used to describe non-selective adsorption of HA on non-imprinted materials and besides the molecular imprints of MIPs. The choice of a combined Langmuir–Volmer model appears an accurate description

of the simultaneous selective and non-selective adsorption of HA on the MIPs, as well as the choice of the Volmer model for the non-selective adsorption of HA on NIPs.

3.2.2.1. The Langmuir–Volmer model

The following equations describe the interaction model between the synthesized materials MIP_4, NIP_4, and HA:

Langmuir model equation

$$Q_s = Q_{max,s} \frac{K_S\, C}{1+K_S\, C} \quad (7)$$

where Q_s (μmol·m^{-2}) is the amount adsorbed at equilibrium, $Q_{max,s}$ (μmol·m^{-2}) is the maximum adsorption capacity for selective sites, C (μmol·L^{-1}) concentration of the solute at equilibrium, and K_S is the binding constant for selective sites.

Volmer model equation

$$C_e = \frac{1}{K_{ns}} \frac{\theta}{1-\theta} e^{\frac{\theta}{1-\theta}} \quad (8)$$

where $\theta = Q/Q_{max,ns}$ is the coverage and K_{ns} is the binding constant for non-selective adsorption. The difference between the Langmuir equation and the Volmer equation is that the affinity remains constant in the Langmuir adsorption mechanism, whereas it decreases with the coverage θ in the Volmer mechanism.

The Volmer isotherm was fitted to the experimental non-selective adsorption isotherms to NIPs by non-linear regression for the two variable parameters, non-selective binding constant K_{ns} and adsorption at full coverage $Q_{max,ns}$ minimizing the absolute relative error (*ARE*, Eq. 9). The non-selective and selective contributions to the experimental adsorption to MIPs was described by the sum of a Langmuir and a Volmer isotherm with four characteristic parameters K_s, $Q_{max,s}$, K_{ns} and Q_{max} for selective and non-selective adsorption [31].

$$ARE = \frac{1}{(N-p)} \sum_{i=1}^{N} \left| Q_{exp,i} - Q_{calc,i} \right| \quad (9)$$

3.2.3. Effect of varying the type of cross-linking agent

The type of cross-linking agent has a significant impact on the performance of the MIP, namely the material morphology, the stabilization of the imprinted cavity, the mechanical stability of the polymer matrix and the complementary interactions with the target molecules (histamine). It is usual considered that an efficient cross-linking agent allows the formation of a very rigid three-dimensional polymer matrix keeping selective microcavities having shape and chemical functions complementary to that of the target, even after its removal. The rigidity of the matrix polymer allows the functions to remain at their optimal position and orientation for optimum recognition. It has also been shown that for chromatography applications, a high degree of cross-linking agent of the imprinted polymer is advantageous to achieve good separations [32]. Sufficient mechanical stability of the polymer is undoubtedly required for applications such as HPLC; some rigidity of polymer matrix is required to preserve the imprinting memory. In the present study, these ideas about the rigidity requirements are studied in more details. Four types of polymers were synthesized by varying the alkyl chain lengths of the cross-linking agent: BA_1, BA_2, BA_4 and BA_6. The structure of the cross-linking agent, particularly the spacer length, plays a key role in increasing the adsorption capacity of the MIP, as observed by comparing MIP_1, MIP_2, MIP_4 and MIP_6 adsorption capacities at different concentrations of HA. Figure 7 shows the experimental adsorption isotherms for MIP_1, NIP_1, MIP_2, NIP_2, MIP_4, NIP_4, MIP_6, and NIP_6 at 298 K pH 5.5, as well as the best fit of the suitable model. The thermodynamic parameters are listed in Table 2.

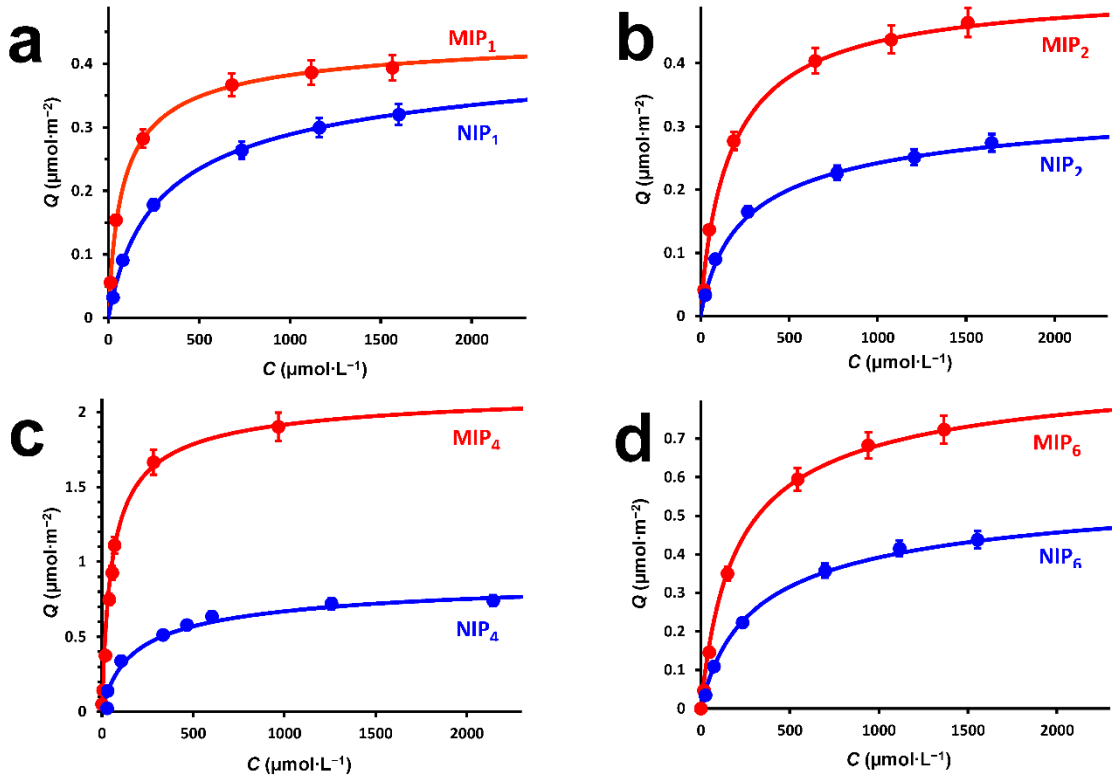

Figure 7. Adsorption isotherms and best fits of the adsorption models to experimental adsorption of HA onto MIP_1 and NIP_1 (a), MIP_2 and NIP_2 (b), MIP_4 and NIP_4 (c), and MIP_6 and NIP_6 (d) at 298 K and pH 5.5.

Table 2. Parameters of the Langmuir–Volmer and Volmer models fitting to HA experimental adsorption isotherms MIP_1 and NIP_1, MIP_2 and NIP_2, MIP_4 and NIP_4, MIP_6 and NIP_6 at 298 K and pH 5.5.

	$Q_{max,s}$ (μmol·m^{-2})	K_s	Log(K_s)	$Q_{max,ns}$ (μmol·m^{-2})	K_{ns}	Log(K_{ns})
MIP_1	0.13	12000	4.08	0.40	11500	4.06
NIP_1				0.58	2700	3.43
MIP_2	0.15	15000	4.18	0.40	5000	3.70
NIP_2				0.47	3200	3.50
MIP_4	1.40	25000	4.40	1.00	5000	3.70
NIP_4				1.20	4500	3.65
MIP_6	0.40	7000	3.85	0.68	2500	3.40
NIP_6				0.80	2500	3.40

The calculated adsorption isotherms matched the experimental data in all instances (Figure 7). Adsorbed amounts to MIP were larger than to NIP, indicating that the MIPs a large contribution of molecular imprints to the adsorption. Furthermore, the adsorption capacity of MIP_4, which

is the sum of $Q_{max,s}$ and $Q_{max,ns}$, was higher than those of the MIP_1, MIP_2 and MIP_6. Therefore, the best-imprinted polymer among the prepared series was MIP_4 due to its highest adsorption capacity and highest difference between the MIP_4 and NIP_4 adsorption capacities. For a HA concentration of 5 ppm, the imprinting factor of MIP_4/NIP_4 pair was IF = 2.5, and the high adsorbed percentage (90 %) demonstrated the efficacy of using the cross-linking agent BA_4 for the synthesis of the polyacrylamide MIP materials. As a comparison under the same conditions, IF = 1.6, 1.4 and 1.4 for the MIP_1/NIP_1, MIP_2/NIP_2 and MIP_6/NIP_6 pairs respectively.

Long spacer and flexibility of the cross-linking agent appear to be beneficial to promote the free radical polymerization around template by improvement of monomer/template interactions in pre-polymerization medium [33]. However, too high flexibility may cause healing of the cavities and the disappearance of molecular imprints [34].

The thermodynamic parameters coming from fitting the adsorption models to the experimental adsorption isotherms provide more specific insight into the physical chemistry of adsorption. Considering the selective part of adsorption to the MIPs, both $Q_{max,s}$ and K_s assumed maximum values for MIP_4. This confirmed to above-mentioned a priori ideas: a moderate flexibility is advantageous, but too much flexibility allows the molecular imprint to irreversibly disappear by healing.

A tentative rationale to the benefits brought about by moderate flexibility considers the formation process of molecular imprints. Cross-linking agents with a short spacer cause the instantaneous formation of a highly rigid network as the polymerization proceeds. There is a need for the HA molecules are present at that time, which requires the presence of a “prepolymerization complex” between HA and the functional monomer (or cross-linker). Such complex species are labile because they are formed by weak interactions. Only the part of the functional monomer associated with HA can cause the formation of molecular imprints. Polymerization and strong cross-linking of the free monomer does not freeze molecular

imprints and the high rigidity prevent further re-arrangement for subsequent binding of HA and delayed formation of molecular imprints. A slight flexibility of the cross-links allows for re-accommodation of the network to the shape and position of functional groups of HA for more HA can bind to the material, thereby increasing the final density of molecular imprints. Regarding the stronger affinity of MIP_4, some flexibility allows for small-scale structural re-arrangements as HA absorbs to the MIP. The stability of the complex species formed during adsorption is therefore better and the affinity constant is higher. Of course, a too high flexibility causes irreversible healing of the molecular imprints and loss of selective adsorption, both regarding the adsorbed amount ($Q_{max,s}$) and the affinity (K_s).

The same phenomena may explain the maximum of $Q_{max,s}$ and K_s for the non-selective adsorption of HA to the MIP besides the molecular imprints and to the NIP. $Q_{max,ns}$ assumed an approximately constant value (0.5 $\mu mol \cdot m^{-2}$) in all cases but MIP_4 and NIP_4. $2500 < K_{ns} < 5000$ is all instances. The higher values of $Q_{max,ns}$ for MIP_4 and NIP_4 may come again from the slight flexibility that allows for rearrangements upon adsorption of HA. Too much flexibility allows the amide functional groups being buried inside the bulk of the polymer material as self-hydrogen-bonded complex species. Indeed, the polymethylene linker of the cross-linking agent BA_6 is preferentially oriented towards the outside because the surface energy of polymethylene (hydrocarbon) is lower than that of polar groups (amide).

3.2.4. Effect of pH

The adsorption behavior depends on the pH for acidic or basic molecules (including histamine) experiencing several ionization states according to the pH [35,36]. It has been assessed at the three pH values of 5.5, 7.4 and 11.4. A strong pH dependence of the surface properties of polyacrylamide is not expected because the neutral primary and secondary amide units of cross-linked polyacrylamide do not have significant acid or basic properties in aqueous medium.

Conversely, the HA molecule experiences several different states in the studied pH range owing to its two p*K*a values of 6.059 and 9.826 [37]. At the strongly basic media of high pH, HA is predominantly in its neutral form. Lowering the pH to 7.4 causes the aliphatic amino group to bind a proton, yielding the singly protonated HA. However, decreasing the pH of the solution will increase the protonation of HA even more. As decreasing the pH again, the imidazole ring can bind a proton, resulting in the formation of the doubly protonated form of HA. At pH 5.5 close to the first p*K*a value, HA is about half singly protonated and half doubly protonated. Figure 8 shows the experimental adsorption isotherms at 298 K for pH 7.4 and 11.4, along with the best fits of the Volmer model to the NIP_4 data and the combined Langmuir–Volmer model for the MIP_4. The parameters of the selective and non-selective adsorption processes provided by the Langmuir–Volmer model for the MIP_4 as well as the parameters for non-selective adsorption found by the Volmer model for the NIP_4 are shown in Table 3.

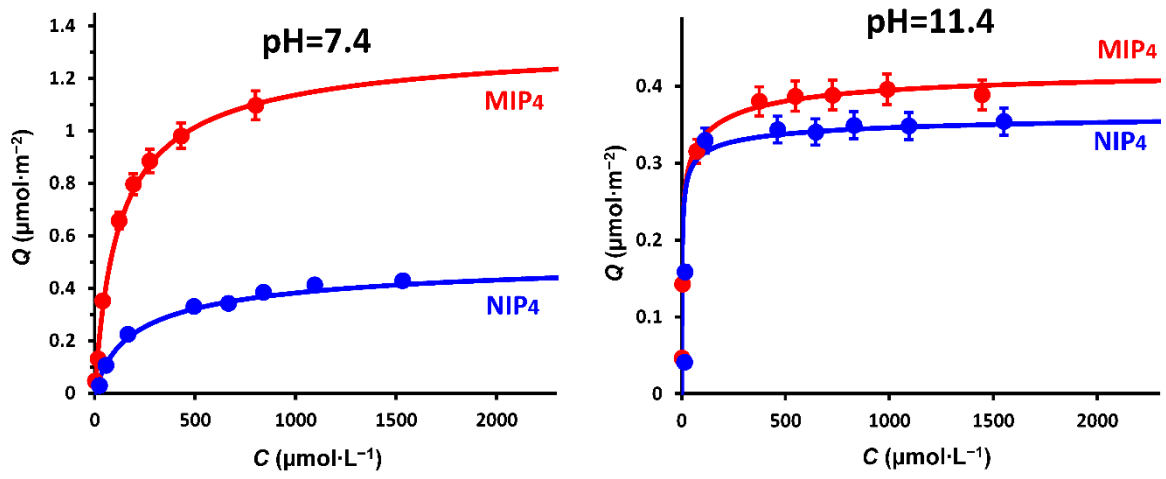

Figure 8. Adsorption isotherms of HA to MIP_4 and NIP_4 at 298 K and pH 7.4 and 11.4.

Table 3. Parameters of the best fits of the Volmer and Langmuir–Volmer models to experimental adsorption isotherms of HA to NIP_4 and MIP_4 at 298 K and various pH.

	NIP_4			MIP_4					
pH	$Q_{max,ns}$ (µmol·m^{-2})	K_{ns}	Log(K_{ns})	$Q_{max,s}$ (µmol·m^{-2})	K_s	Log(K_s)	$Q_{max,ns}$ (µmol·m^{-2})	K_{ns}	Log(K_{ns})

5.5	1.20	4500	3.65	1.40	25000	4.40	1.00	5000	3.70
7.4	0.70	4000	3.60	0.83	10000	4.00	0.70	4000	3.60
11.4	0.42	500000	5.70	0.057	6000	3.78	0.42	500000	5.70

Adsorption was stronger at pH 5.5 than 7.4, showing that the protonated form of HA has a stronger affinity for amide functional groups. The acidic ammonium groups bind to the basic carbonyl of amide functional groups by hydrogen bonds. Selective adsorption to molecular imprints may rely on a kind of shape memory, but much more probably the presence of several functional groups with optimum position and orientation allowing for multiple hydrogen bonding interactions with HA. A doubly protonated form of HA allows for the formation of two hydrogen bonds with two different basic sites in the same molecular imprint. The adsorption isotherm measured at pH 11.4 looks in contradiction with this picture because of the reproducible very steep increase of adsorbed amounts for low concentrations of HA. Therefore, the affinity constant was very high. The maximum adsorbed amounts $Q_{max,s}$ and $Q_{max,ns}$ were lower than at pH 5.5 and 7.4 according to the trend. Indeed, the fast hydrolysis of the amide groups into carboxylic salts may be the origin of such a behavior. Indeed, such hydrolysis is well-documented for the water-soluble polyacrylamide [38,39]. The low adsorbed amount of HA that marks a low density of functional groups may correspond to a low level of hydrolysis. Hydrolysis taking place at random on the surface of the material does not form molecular imprints, so that the difference between the MIP and NIP vanishes at pH 11.4 (Figure 8).

3.2.5. Enthalpic and entropic contributions to the standard free energy of adsorption

The association equilibrium constants K_s and K_{ns} measured at pH = 5.5 and various temperatures (298 K, 313 K, 323 K and 333 K) were used to estimate the thermodynamic parameters of the adsorption process such as the standard Gibbs free enthalpy $\Delta_{ads}G^0$, standard enthalpy $\Delta_{ads}H^0$, and standard entropy $\Delta_{ads}S^0$. The Langmuir–Volmer model was used to model the adsorption

isotherms in the same way as for the part on the influence of pH, and these constants were determined for each type of adsorption to the imprinted polymer MIP_4 (Figure S7). These thermodynamic parameters have been determined from the van't Hoff equation shown below:

$$\ln(K_a) = \frac{\Delta_{ads}S_a^0}{R} - \frac{\Delta_{ads}H_a^0}{RT} \quad (9)$$

where K_a is the temperature-dependent association equilibrium constant for selective adsorption $K_a = K_s$ or non-selective adsorption $K_a = K_{ns}$, T is the temperature and R is the gas constant (8.314 $J{\cdot}mol^{-1}{\cdot}K^{-1}$). The plot of $Log(K_a)$ as a function of $10^3/T$ allows the calculation of $\Delta_{ads}H^0$ (slope) and $\Delta_{ads}S^0$ (y-intercept) (Figure 9). These plots were linear, showing that $\Delta_{ads}H^0$ and $\Delta_{ads}S^0$ did not depend on temperature in the temperature range studied. Table 4 summarizes the values of the thermodynamic parameters of each adsorption process. The thermodynamic parameters for the adsorption of HA to the NIP were identical to those of the non-selective adsorption to the MIP.

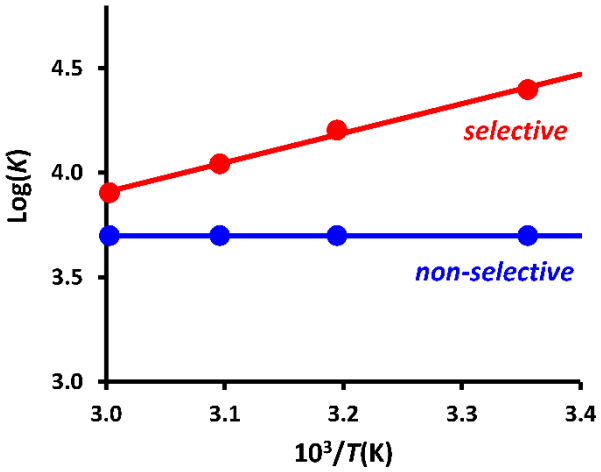

Figure 9. Variation of $Log(K_a)$ as a function of $10^3/T$ for the selective (red) and non-selective (blue) adsorption of HA on the imprinted material MIP_4.

Table 4. Thermodynamic parameters of the selective and non-selective adsorption of HA on the imprinted material MIP_4, $\Delta_{ads}H^0$, $\Delta_{ads}S^0$, and $\Delta_{ads}G^0$ at 298 K.

MIP_4	**$\Delta_{ads}H^0$ ($kJ{\cdot}mol^{-1}$)**	**$\Delta_{ads}S^0$ ($J{\cdot}mol^{-1}{\cdot}K^{-1}$)**	**$\Delta_{ads}G^0$ ($kJ{\cdot}mol^{-1}$)**
Selective sites	−27.0	−6.2	−25.1
Non-selective areas	0.0	70.9	−21.1

The Gibbs free enthalpies $\Delta_{ads}G^0$ at 298 K were obviously negative for all adsorption processes because the adsorption of HA is spontaneous. $\Delta_{ads}G^0$ is also negative for MIP_4 and NIP_4 at the other temperatures (Table S3). Non-selective adsorption to the imprinted polymer was athermal ($\Delta_{ads}H^0 \approx 0$). The adsorption of HA on the selective sites of the imprinted polymer was exothermic ($\Delta_{ads}H^0 < 0$). The adsorption of the HA molecules to molecular imprints was an entropy-controlled process [40]. Several types of interactions are operating adsorption with either positive or negative enthalpies. The total standard enthalpy may assume positive or negative values depending of the balance of all interaction enthalpies. Hydrogen-bonding interactions are not athermal, so that an athermal balance obviously is the result of a compensation of positive and negative contributions. Restricting the discussion to hydrogen bonding interactions only, the exothermic process of binding of HA to molecular imprints or besides them is necessarily accompanied by release of water molecules that were hydrogen-bonded to the polymer and to free HA. These dehydration processes are endothermic. Molecular imprints include several functional groups for being efficient at selective recognition of the guest molecules [41,42], so that it is presumed that HA molecules bind to molecular imprints by several hydrogen bonds. This is the reason why HA has a selective adsorption to molecular imprints. The origin of binding of HA to the MIP area besides molecular imprints also involves hydrogen bonds, but the random position and orientation of the functional groups of the polymer does not allow multiple hydrogen-bonding interactions per HA molecule. The bonds of HA to the polymer at and off the molecular imprints are different; this is revealed by their different values of $\Delta_{ads}H^0$. The large increase of standard entropy for adsorption to molecular imprints is also rationalized on the same grounds. Binding to molecular imprints by means of several hydrogen bonds per HA molecule releases several free water molecules; the balance of the number of free molecules increases, so that the entropy increases.

3.2.6. Kinetics of adsorption

The adsorption kinetics of HA on MIP_4 (Figure 10) was fast since 90 % of equilibrium binding took place in the first 5 min for all HA concentrations. Adsorption equilibrium was reached in approximately 20 min. Adsorption to NIP_4 was fast, but much less than the MIP_4 material, which was expected because the non-imprinted polymer did not contain molecular imprints for selective adsorption of HA. In the framework of applications to HA analysis such as sample pre-concentration in solid-phase microextraction devices (SPME), fast adsorption is an extremely important parameter to enable large flow rates and short analysis times [43].

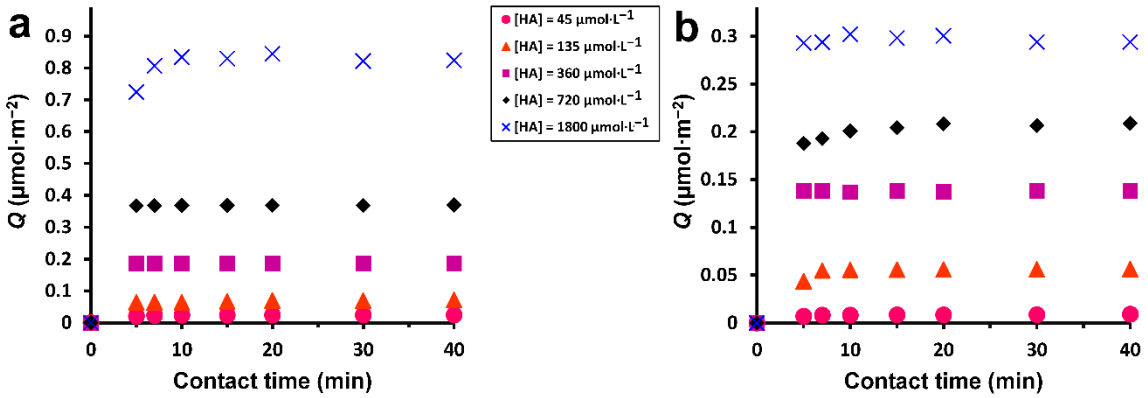

Figure 10. Kinetics of HA adsorption on MIP_4 (a) and NIP_4 (b) for five HA concentrations at pH 5.5.

3.2.7. Selectivity study

Competitive adsorption tests were carried out in an aqueous solution comprising mixes of HA and its structural analogs MEL and TYR to determine the selectivity of the synthesized compounds. The calibration curves and the chromatograms of MEL and TYR are given in section S.6 of Supporting Information. In comparison to the other two samples, a considerable decrease was found as indicated in Figure 11 due to the interaction of the polymer and HA. The adsorption capacity of MIP_4 and NIP_4 toward HA was significantly higher than that of its analogs. Furthermore, a comparison of adsorption capabilities of the imprinted and non-imprinted polymers for each component shows that MIP_4 has greater selectivity for HA molecules. Furthermore, the imprinting factor, $IF = Q(\text{MIP})/Q(\text{NIP})$, was used to infer the

selectivity of MIP_4. The *IF* of HA was 2.46, whereas *IF*'s respectively were 1.0 and 1.16 for the MEL and TYR analogs. On this basis, significant selective adsorption was only observed for HA. The selectivity coefficient α and distribution coefficient *D* (Table 5) of MIP_4 toward HA were greater than those of NIP_4. Such findings provide a clear demonstration of the high selectivity of MIP_4 toward HA. It is worth noticing that HA and MEL showed the same non-selective binding to NIP_4, but HA showed a definitely higher binding to molecular imprints of MIP_4. The selectivity toward HA is associated with the imprinting effect, in which the recognition of the MIP_4 particles is dominated by molecular size, structure, and the position/orientation memory of functional groups.

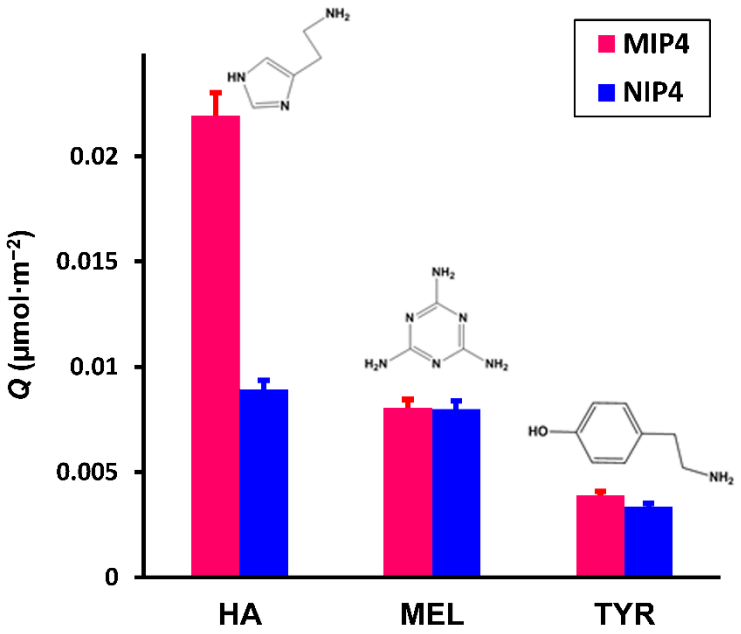

Figure 11. Binding capacities for MIP_4 and NIP_4 for HA, MEL, and TYR.

Table 5. Competitive sorption of HA, MEL and TYR on MIP_4 and NIP_4 sorbents.

	MIP_4		**NIP_4**	
Compound	*D* ($L \cdot m^{-2}$)	α	*D* ($L \cdot m^{-2}$)	α
HA	1.47	–	0.095	–
TYR	0.03	46.3	0.026	3.6
MEL	0.08	17.9	0.080	1.2

4. Conclusion

The investigation of the influence of cross-linking agents flexibility on the properties of MIPs showed that the requirement for a very high rigidity may be advantageously released. Indeed, the BA_4 cross-linking agent having a four methylenes spacer linking the two acrylamide groups was optimum regarding the binding capacity and selective binding of histamine. Fast adsorption kinetics and excellent adsorption efficiency for HA were reported, revealing the favorable performance of MIP_4 as cross-linking agent. The higher adsorption capacity of the MIP_4 compared to the NIP_4 at optimal experimental conditions (pH = 5.5, T = 298 K) provided evidence of selective HA binding. Investigation of the adsorption thermodynamics revealed the different features of the adsorption at molecular imprints and off them: adsorption to molecular imprints is exothermic whereas that besides them is athermal. Finally, the selectivity against interfering molecules has successfully demonstrated that HA imprinting has a higher *IF* when compared to the other analogs. The present results go against the common idea that a very rigid material is mandatory. The picture that emerges from the present work is that a moderate flexibility of the cross-links is advantageous. The empty molecular imprints may heal once the template has been removed. But the flexibility of the material allows them to open again in the presence of the adsorbing molecules for the molecular imprints fit their guest. Too much flexibility makes the healing process irreversible; moderate healing allows reversible structural rearrangements for both the empty and the filled molecular imprints reach their state of minimal free energy. The common idea of the necessary structural freezing of the molecular imprints structure by tight and rigid cross-linking has been recently questioned by considering the different steps during the polymerization reaction that finally yields the MIP material [44]. The outcome of the present study agrees with the conclusion of this latter interesting work, though the present study addressed the final selective adsorption properties better than the intermediate structures encountered during the polymerization course.

The successful synthesis of highly selective MIP for HA using a new tetramethylene spacer cross-linker (BA_4) is a clue to prospects for a large number of applications. Regarding applications in pharmacy and medicine, the use for selective binding of active substances and drug delivery, the selective capture of biological materials and in analytical chemistry such as application in SPME.

Acknowledgment

This work was supported by the "PHC Utique" program for French–Tunisian cooperation (project number 19G1204).

[1] B. Sellergren (ed.). *Molecularly Imprinted Polymers. Man-made Mimics of Antibodies and their Applications in Analytical Chemistry*. Elsevier, Amsterdam (2001).
[2] C. Alvarez-Lorenzo, A. Concheiro (eds). *Handbook of Molecularly Imprinted Polymers*, Smithers Rapra, Shawbury (2013).
[3] S. Li, Y. Ge, A.A. Piletsky, J. Lunec (eds). *Molecularly Imprinted Sensors: Overview and Applications*, Elsevier, Amsterdam (2012).
[4] S. Li, S. Cao, S.A. Piletsky, A.P.F. Turner (eds). *Molecularly Imprinted Catalysts. Principles, Syntheses, and Applications*, Elsevier, Amsterdam (2016).
[5] B. Mattiasson, L. Ye (eds). *Molecularly Imprinted Polymers in Biotechnology*, Advances in Biochemical Engineering/Biotechnology Vol. 150, Springer, Heidelberg (2015).
[6] I.A. Nicholls, K. Adbo, H.S. Andersson, P.O. Andersson, J. Ankarloo, J. Hedin-Dahlström, P. Jokela, J.G. Karlsson, L. Olofsson, J. Rosengren, S. Shoravi, J. Svenson, S. Wikman, Can we rationally design molecularly imprinted polymers? Anal. Chim. Acta 435 (2001) 9–18, doi:10.1016/S0003-2670(01)00932-1.
[7] L.E. Nielsen, Cross-linking–effect on physical properties of polymers, J. Macromol. Sci., Part C 3 (1969) 69–103, doi:10.1080/15583726908545897.
[8] B. Sellergren (ed.). *Molecularly Imprinted Polymers. Man-made Mimics of Antibodies and their Applications in Analytical Chemistry*. Elsevier, Amsterdam (2001), pp. 41–42.
[9] T. Muhammad, Z. Nur, E.V. Piletska, O. Yimit, S.A. Piletsky, Rational design of molecularly imprinted polymer: the choice of cross-linker, Analyst, 137 (2012), 2623–2628, doi:10.1039/c2an35228a.
[10] B. Sellergren, Molecular imprinting by noncovalent interactions: Enantioselectivity and binding capacity of polymers prepared under conditions favoring the formation of template complexes, Makromol. Chem. 190 (1989) 2703–2711, doi:10.1002/macp.1989.021901104.
[11] K. da Mata, M. Zanetti Corazza, F. Midori de Oliveira, A.L. de Toffoli, C.R. Teixeira Tarley, A. Benedito Moreira, Synthesis and characterization of cross-linked molecularly imprinted polyacrylamide for the extraction/preconcentration of glyphosate and aminomethylphosphonic acid from water samples, React. Funct. Polym. 83 (2014) 76–83, doi:10.1016/j.reactfunctpolym.2014.07.004.
[12] C.-Y. Hung, Y.-T. Huang, H.-H. Huang, C.-C. Hwang, Sulfamethazine and sulfadimethoxine separation strategies based on molecularly imprinted adsorbents, Anal. Lett. 40 (2007) 3232–3244, doi:10.1080/00032710701672707.
[13] X. Shi, Y. Meng, J. Liu, A. Sun, D. Li, C. Yao, Y. Lu, J. Chen, Group-selective molecularly imprinted polymer solid-phase extraction for the simultaneous determination of six sulfonamides in aquaculture products, J. Chromatogr. B, 879 (2011) 1071–1076, doi:10.1016/j.jchromb.2011.03.019.

[14] L.A. Tom, N.A. Schneck, C. Walter, Improving the imprinting effect by optimizing template:monomer:cross-linker ratios in a molecularly imprinted polymer for sulfadimethoxine, J. Chromatogr. B 909 (2012) 61–64, doi:10.1016/j.jchromb.2012.10.020.
[15] O.A. Pisarev, I.V. Polyakova, Molecularly imprinted polymers based on methacrylic acid and ethyleneglycol dimethacrylate for L-lysine recognition, React. Funct. Polym. 130 (2018) 98–110, doi:10.1016/j.reactfunctpolym.2018.06.002.
[16] R.P. Kennan, K.A. Richardson, J. Zhong, M.J. Maryanski, J.C. Gore, The effects of cross-link density and chemical exchange on magnetization transfer in polyacrylamide gels, J. Magn. Reson. Ser B 110 (1996) 267–277, doi:10.1006/jmrb.1996.0042.
[17] M.P. Davies, V. De Biasi, D. Perrett, Approaches to the rational design of molecularly imprinted polymers, Anal. Chim. Acta 504 (2004) 7–14, doi:10.1016/S0003-2670(03)00812-2.
[18] F. Navarro-Villoslada, B. San Vicente, M.C. Moreno-Bondi, Application of multivariate analysis to the screening of molecularly imprinted polymers for bisphenol A, Anal. Chim. Acta 504 (2004) 149–162, doi:10.1016/S0003-2670(03)00766-9.
[19] C. Yu, K. Mosbach, Molecular imprinting utilizing an amide functional group for hydrogen bonding leading to highly efficient polymers, J. Org. Chem. 62 (1997) 4057–4064, doi:10.1021/jo961784v.
[20] M. Boukadida, A. Anene, N. Jaoued-Grayaa, Y. Chevalier, S. Hbaieb, Choice of the functional monomer of molecularly imprinted polymers: Does it rely on strong acid-base or hydrogen bonding interactions ?, Colloid Interface Sci. Commun. 50 (2022) 100669, doi:10.1016/j.colcom.2022.100669.
[21] A. Noomane, S. Hbaieb, M.-A. Bolzinger, S. Briançon, Y. Chevalier, R. Kalfat, Effectiveness of grafting modes of methoxycinnamate sunscreen onto silica particles, Colloids Surfaces A: Physicochem. Eng. Aspects 441 (2014) 653–663, doi:10.1016/j.colsurfa.2013.10.029.
[22] S. Kouki, N. Jaoued-Grayaa, A. Anene, E. Beyou, Y. Chevalier, S. Hbaieb, The enhanced adsorption properties of molecular imprinted polymer material prepared using nitroxide-mediated Radical Deactivation Reversible Polymerization, Polymer 249 (2022) 124841, doi:10.1016/j.polymer.2022.124841.
[23] S. Azodi-Deilami, M. Abdouss, D. Kordestani, Synthesis and characterization of the magnetic molecularly imprinted polymer nanoparticles using *N*,*N*-bis-methacryloyl ethylenediamine as a new cross-linking agent for controlled release of meloxicam, Appl. Biochem. Biotechnol. 172 (2014) 3271–3286, doi:10.1007/s12010-014-0769-6.
[24] S.B. Rodrigues, F.M. Collares, D. Gamba, V.C.B. Leitune, C.L. Petzhold, Thermal radical polymerization of bis(methacrylamide)s, Polímeros 29 (2019) e2019023, doi:10.1590/0104-1428.03218.
[25] M. Dimitrijevic, S. Stefanovic, N. Karabasil, D. Vasilev, N. Cobanovic, N. Ilic, V. Djordjevic, UPLC-MS/MS determination of histamine levels in canned fish collected from Belgrade retail markets, Meat Technol. 57 (2016) 47–56, http://www.journalmeattechnology.com/index.php/meat_technology/article/view/38.
[26] A. Anene, K. Hosni, Y. Chevalier, R. Kalfat, S. Hbaieb, Molecularly imprinted polymer for extraction of patulin in apple juice samples, Food Control 70 (2016) 90–95, doi:10.1016/j.foodcont.2016.05.042.
[27] C. Ayadi, A. Anene, R. Kalfat, Y. Chevalier, S. Hbaieb, Molecularly imprinted polyaniline on silica support for the selective adsorption of benzophenone-4 from aqueous media, Colloids Surfaces A: Physicochem. Eng. Aspects 567 (2019) 32–42, doi:10.1016/j.colsurfa.2019.01.042.
[28] E. Abdollahic, A. Khalafi-Nezhad, A. Mohammadi, M. Abdouss, M. Salami-Kalajahi, Synthesis of new molecularly imprinted polymer via reversible addition fragmentation transfer polymerization as a drug delivery system, Polymer 143 (2018) 245–257, doi:10.1016/j.polymer.2018.03.058.
[29] A. Anene, R. Kalfat, Y. Chevalier, S. Hbaieb, Design of molecularly imprinted polymeric materials: The crucial choice of functional monomers, Chem. Africa 3 (2020) 769–781, doi:10.1007/s42250-020-00180-1.
[30] M. Thommes, K. Kaneko, A.V. Neimark, J.P. Olivier, F. Rodriguez-Reinoso, J. Rouquerol, K.S.W. Sing, Physisorption of gases, with special reference to the evaluation of surface area and pore size distribution (IUPAC Technical Report). Pure Appl. Chem. 87 (2015) 1051–1069, doi:10.1515/pac-2014-1117.
[31] C. Ayadi, A. Anene, R. Kalfat, Y. Chevalier, S. Hbaieb, Molecular imprints frozen by strong intermolecular interactions in place of cross-linking, Chem. Eur. J. 27 (2021) 2175–2183, doi:10.1002/chem.202004580.
[32] I. Iturralde, M. Paulis, J.R. Leiza, The effect of the cross-linking agent on the performance of propranolol imprinted polymers, Eur. Polym. J. 53 (2014) 282–291, doi:10.1016/j.eurpolymj.2014.02.003.
[33] E. Yilmaz, K. Mosbach, K. Haupt, Influence of functional and cross-linking monomers and the amount of template on the performance of molecularly imprinted polymers in binding assays, Anal. Commun. 36 (1999) 167–170, doi:10.1039/a901339c.
[34] D.L. Safranski, K. Gall, Effect of chemical structure and cross-linking density on the thermo-mechanical properties and toughness of (meth)acrylate shape memory polymer networks, Polymer 49 (2008) 4446–4455, doi:10.1016/j.polymer.2008.07.060.

[35] M. Hashemi, Z. Nazari, N. Noshirvani, Synthesis of chitosan-based magnetic molecularly imprinted polymers for selective separation and spectrophotometric determination of histamine in tuna fish, Carbohydr. Polym. 177 (2017) 306–314, doi:10.1016/j.carbpol.2017.08.056.
[36] E. Öngün, S. Akgönüllü, H. Yavuz, A. Denizli, Synthesis of molecularly imprinted magnetic nanoparticles for selective cytidine adsorption, Sep. Sci. Plus 4 (2021) 147–156, doi:10.1002/sscp.202000089.
[37] W.J. Eilbeck, F. Holmes, T.W. Thomas, Metal complexes of histamine [4(5)-(2-aminoethyl)imidazole] and isohistamine [2-(2-aminoethyl)imidazole], J. Chem. Soc. (A) (1969) 113–115, doi:10.1039/J19690000113.
[38] K. Nagase, K. Sakaguchi, Alkaline hydrolysis of polyacrylamide, J. Polym. Sci.: Part A 3 (1965) 2475–2482, doi:10.1002/pol.1965.100030706.
[39] V.F. Kurenkov, H.-G. Hartan, F.I. Lobanov, Alkaline hydrolysis of polyacrylamide, Russian J. Appl. Chem. 74 (2001) 543–554, doi:10.1023/A:1012786826774.
[40] V.P. Joshi, M.G. Kulkarni, R.A. Mashelkar, Enhancing adsorptive separations by molecularly imprinted polymers: Role of imprinting techniques and system parameters, Chem. Eng. Sci. 55 (2000) 1509–1522, doi:10.1016/S0009-2509(99)00419-4.
[41] R. Horikawa, H. Sunayama, Y. Kitayama, E. Takano, T. Takeuchi, A programmable signaling molecular recognition nanocavity prepared by molecular imprinting and post-imprinting modifications, Angew. Chem. Int. Ed. 55 (2016) 13023–13027, doi:10.1002/anie.201605992.
[42] T. Curk, J. Dobnikar, D. Frenkel, Rational design of molecularly imprinted polymers, Soft Matter 12 (2016) 35−44, doi:10.1039/c5sm02144h.
[43] S. Asman, S. Mohamad, N.M. Sarih, Study of the morphology and the adsorption behavior of molecularly imprinted polymers prepared by reversible addition-fragmentation chain transfer (RAFT) polymerization process based on two functionalized β-cyclodextrin as monomers, J. Mol. Liquids 214 (2016) 59–69, doi:10.1016/j.molliq.2015.11.057.
[44] T. Cowen, E. Stefanucci, E. Piletska, G. Marrazza, F. Canfarotta, S.A. Piletsky, Synthetic mechanism of molecular imprinting at the solid phase, Macromolecules 53 (2020) 1435−1442, doi:10.1021/acs.macromol.9b01913.

SUPPORTING INFORMATION

Effect of cross-linking agents on the adsorption of histamine on molecularly imprinted polyacrylamide

Merymene Boukadida[a,b], Najeh Jaoued-Grayaa[c], Amira Anene[c], Yves Chevalier[a,*], Souhaira Hbaieb[b,*]

[a] Laboratoire d'Automatique, de Génie des Procédés et de Génie Pharmaceutique, Université de Lyon 1, UMR 5007 CNRS, 69622 Villeurbanne Cedex, France.
[b] Laboratoire de Recherche: Caractérisations, Applications et Modélisation de Matériaux, Université de Tunis El Manar, Faculté des Sciences de Tunis, Campus universitaire El Manar, Tunisia.
[c] Unité Spécialisée de développement des techniques analytiques, Institut National de Recherche et d'Analyse Physico-chimique, Biotechpole Sidi-Thabet, 2020 Ariana, Tunisia.

S.1. Characterization of the modified silica

The starting modified silica was analyzed by ATR-FTIR spectroscopy. Fig. S1 depicts the IR spectrum for the modified silica SiO_2(APTESMA), which reveals the presence of an intense absorption band of the SiO_2 group as well as the characteristic bands resulting from chemical grafting. They were assigned according detailed charts given in the book of Socrates [1].

The N–H stretching vibrations of the secondary amide group and the ν_{SiO-H} stretching vibrations of residual surface silanols (only a part of them participated to the grafting reaction) were observed as a broad band in the range 3500–3200 cm^{-1}. The C–H stretching vibrations of CH_2 and CH_3 coming from the organic graft appeared as a broad band in the 3100–2850 cm^{-1} range. This composite band includes the stretching vibrations of CH_3 (ν_{asym} at 2975–2950 cm^{-1} and ν_{sym} at 2885–2865 cm^{-1}) and CH_2 (ν_{asym} at 2940–2915 cm^{-1}, ν_{sym} at 2870–2840 cm^{-1} and 3 bands of =C–H stretching at 3150–2930 cm^{-1}). An overtone of the amide II band is located in the gap between the O–H/N–H and C–H stretching bands (3100–3070 cm^{-1}). Evidence of binding of the methacryloyl amide was given by the characteristic band of secondary amide stretching vibrations $\nu_{C=O}$ at 1605 cm^{-1} and amide II (δ_{N-H} and ν_{C-N}) bands at 1570–1510 cm^{-1}. The stretching vibrations of the vinyl double bond $\nu_{C=C}$ conjugated with the carbonyl appeared in the same spectral region (1660–1580 cm^{-1}). A very intense absorption at 1100–1000 cm^{-1} corresponded to the Si–O–Si stretching vibrations of silica.

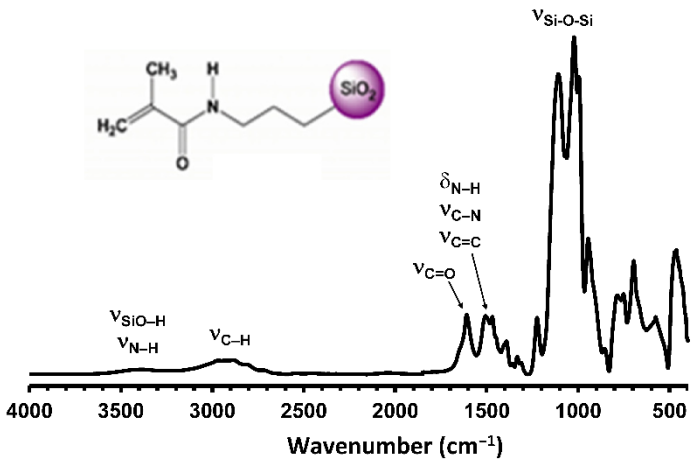

Figure S1. IR spectrum of SiO_2(APTESMA).

The CP-MAS ^{13}C NMR analysis of SiO_2(APTESMA) (Fig. S2) clearly showed the presence of the characteristic peaks corresponding to the carbon atoms of the organic part grafted to the silica surface. The peaks of the –C=O, –C=CH_2, –C=CH_2, –CH_2–NH–, –CH_3 and –NH–CH_2–CH_2–CH_2– groups of APTESMA immobilized on the surface of the silica were observed at 182.99, 142.55, 104.55, 46.76–43.70, 24.13–18.51 and 11.48 ppm, respectively [2].

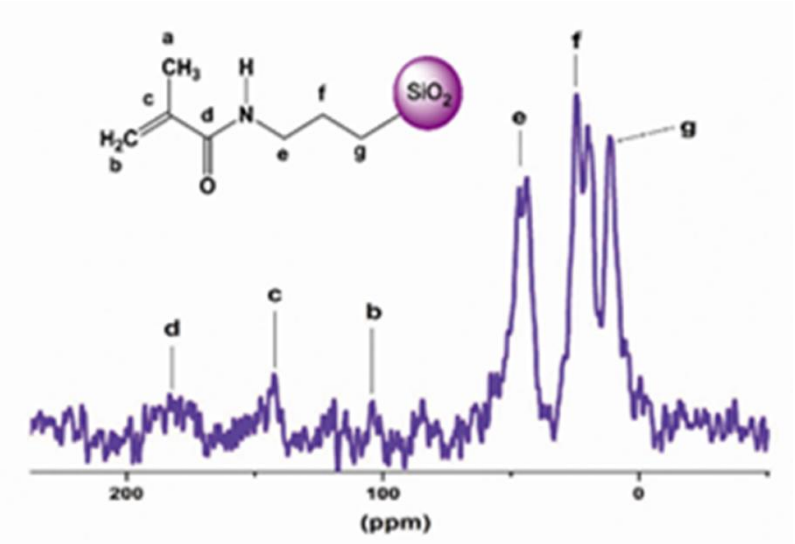

Figure S2. CP-MAS ^{13}C NMR spectrum of SiO_2(APTESMA).

The CP-MAS ^{29}Si NMR spectrum confirmed that silica has been successfully functionalized with APTESMA. The signals corresponding to the silane groups Q^4[$Si(OSi)_4$], Q^3[$Si(OSi)_3OH$], and Q^2[$Si(OSi)_2(OH)_2$] (Fig. S3) of the modified silica SiO_2(APTESMA) have chemical shifts at −109.44, −106.54, and −99.40 ppm, respectively. Three other peaks T^1, T^2 and T^3 were observed at −47.67, −58.05 and 64.95 ppm in the same spectrum. The T^3 sites are attributed to the silicon atom of APTES forming three siloxane bonds with the silicon atom of silica and one bond with the carbon of the propyl chain. The T^2 sites involve the formation of two siloxane bonds with silica and a Si–OH bond corresponding to a hydrolyzed ethoxysilyl group of the triethoxysilane. The T^1 sites correspond to silane bound to silica by only one Si–O–Si linkage, leaving two ethoxysilyl group that were hydrolyzed into two Si–OH groups.

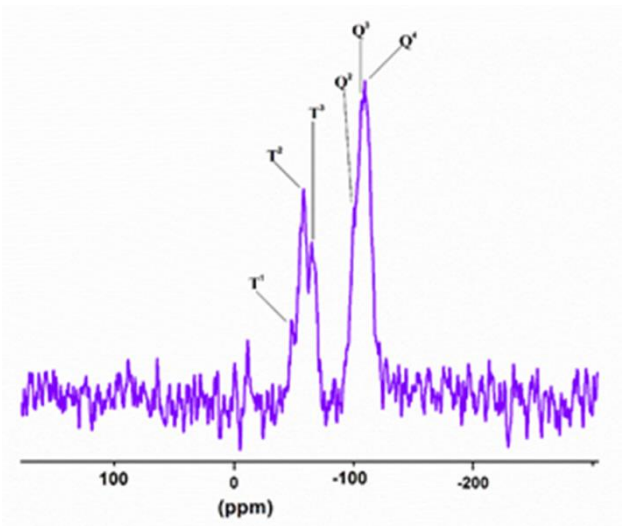

Figure S3. CP-MAS ^{29}Si NMR spectrum of silica SiO_2(APTESMA).

The grafting density of SiO_2(APTESMA) was assessed by thermogravimetric analysis (Fig. S4). The condensation of unreacted Si–OEt groups and their hydrolyzed form (Si–OH), together with the amount of water adsorbed on the silica surface are responsible for the first mass loss at 200 °C. A second mass loss between 350 °C and 600 °C corresponded to the decomposition of the organic materials grafted to the silica surface.

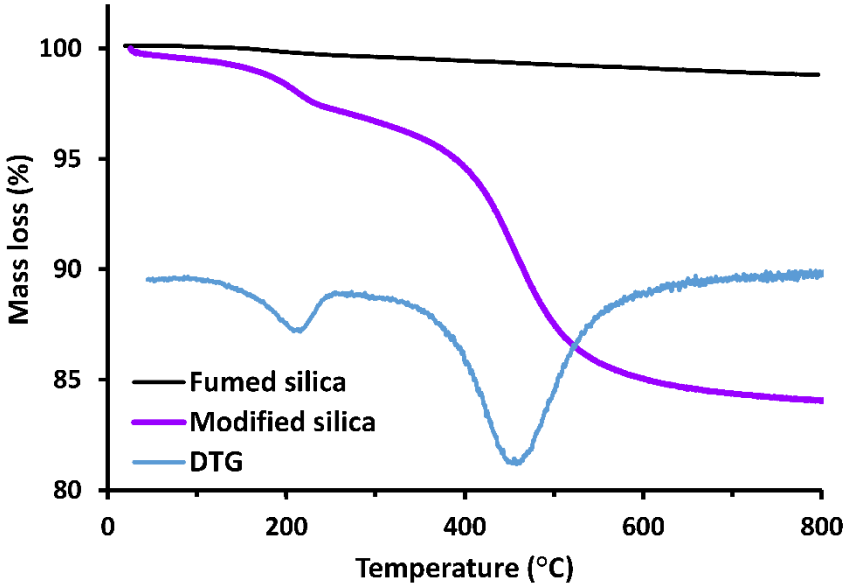

Figure S4. Thermogravimetric analyses of SiO_2(APTESMA) and starting fumed silica. DTG is the derivative of the mass loss of modified silica with respect to temperature.

The grafting density was calculated using the mass loss $m(SiO_2\text{-APTESMA})$ corresponding to the thermal decomposition of the organic graft occurring between 350 °C and 600 °C using Eq. S1 [3].

$$d(\mu mol \cdot m^{-2}) = \frac{\frac{m(SiO2-APTESMA)}{100-m(SiO2-APTESMA)} - \frac{m(SiO_2)}{100}}{M_{mol}(APTESMA) \times A_{SP}} \times 10^6 \qquad \text{Eq. S1}$$

$m(SiO_2\text{-APTESMA})/100$ was the mass loss relative to the mass of the full material; it was converted into the mass loss relative to the mass of silica by dividing it by $1 - m(SiO_2\text{-APTESMA})/100$. This quantity was corrected for the mass loss coming from the dehydration of surface silanols by subtracting the mass loss $m(SiO_2)/100$ of the bare starting silica relative to the mass of silica measured in the same temperature range. The surface density of organic grafts expressed in $mol \cdot m^{-2}$ was calculated by dividing the latter mass of organic graft per mass of silica by the molar mass of the propylmethacrylamide moiety ($C_7H_{12}NO$) lost upon thermal degradation, M_{mol}(APTESMA) = 126 $g \cdot mol^{-1}$, and the specific surface area of silica, A_{SP} = 200 $m^2 \cdot g^{-1}$. The experimental values $m(SiO_2\text{-APTESMA})$ = 14.2% and $m(SiO_2)$ = 0.9% yielded d = 6.21 $\mu mol \cdot m^{-2}$.

The grafting density was also determined by elemental analysis of carbon and nitrogen as:

$$d(\mu mol \cdot m^{-2}) = \frac{1}{A_{SP}} \frac{1}{\frac{100 \times 12 \times n_C}{\%C} - 1} \times 10^6 \qquad \text{Eq. S2}$$

$$d(\mu mol \cdot m^{-2}) = \frac{1}{A_{SP}} \frac{1}{\frac{100 \times 14 \times n_N}{\%N} - 1} \times 10^6 \qquad \text{Eq. S3}$$

where n_C and n_N are the numbers of carbon and nitrogen atoms in the graft; A_{SP} is the specific surface area of silica (200 $m^2 \cdot g^{-1}$); %C and %N are the percentages of carbon and nitrogen determined from elemental analyses. The grafting densities coming from the two elemental analyses were in accordance with those calculated from thermogravimetric analyses (Table S1).

Table S1. Determination of the surface grafting densities of the modified silica from elemental analyses (EA) and thermogravimetric analysis.

Material	**Elemental analysis (%)**		**Surface density (µmol·m^{-2})**		
			from EA		**from TGA**
	C	**N**	**C**	**N**	
SiO_2(APTESMA)	10.80	1.75	6.44	6.26	6.21

S.2. TGA determination of the polymer content of MIPs and NIPs

The mass fraction of organic polymer was determined by TGA from the mass loss between 200 and 500 °C [4]. The mass losses were estimated in the TGA records as the vertical distance between tangents to the curves at temperatures below 200 °C and above 500 °C (Fig. S5).

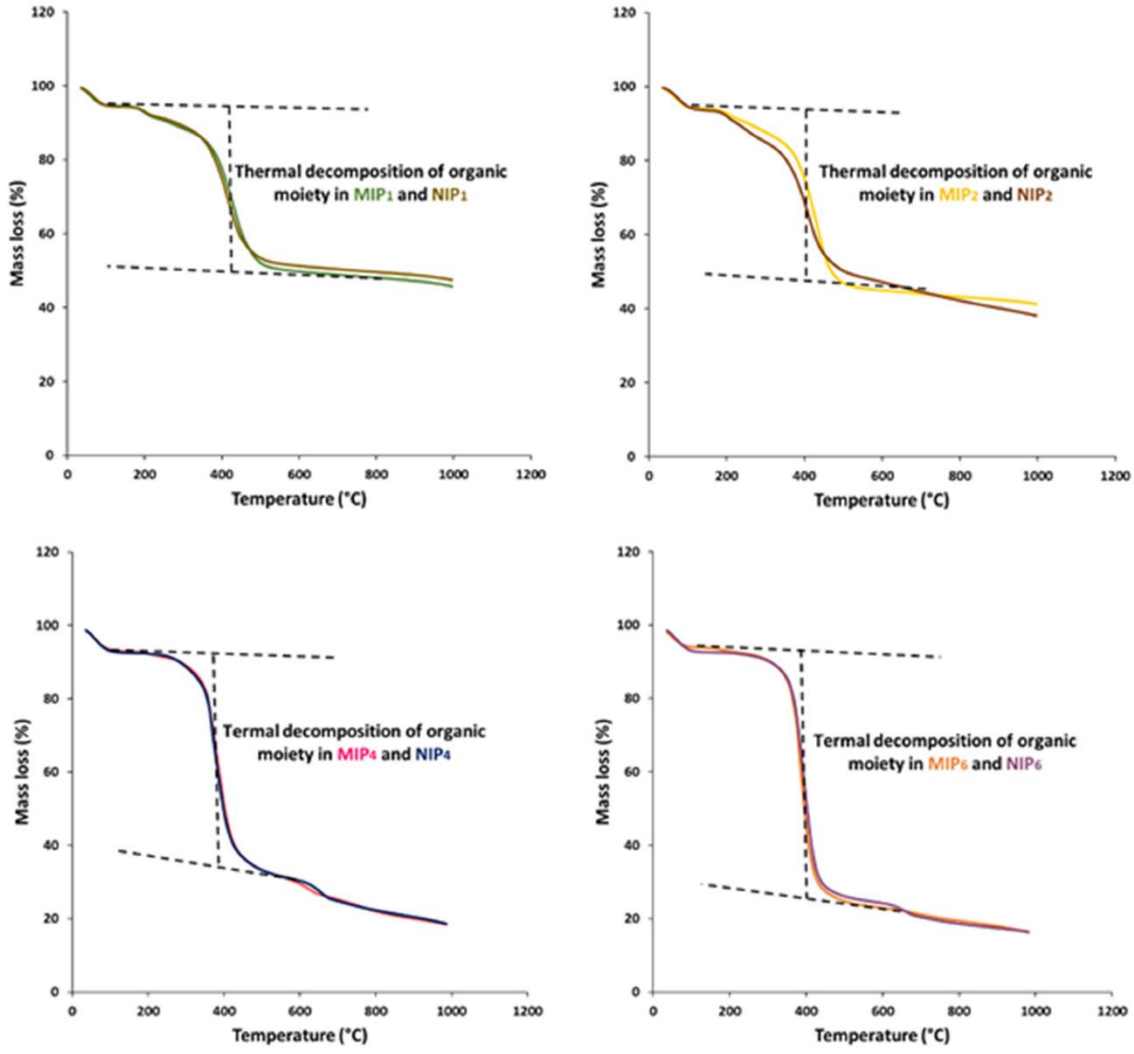

Figure S5. Superimposition of the thermograms of the four synthesized MIPs and NIPs.

S.3. Determination of the specific surface area by BET measurements

The nitrogen gas adsorption and desorption measurements of BET experiments are given in Fig. S6. The adsorption isotherms were of the Type II of the IUPAC classification [5]. The specific surface area was determined from the BET equation fitted to the adsorption data for relative pressures below $p/p_0 = 0.3$. The specific surface areas are given in Table S2.

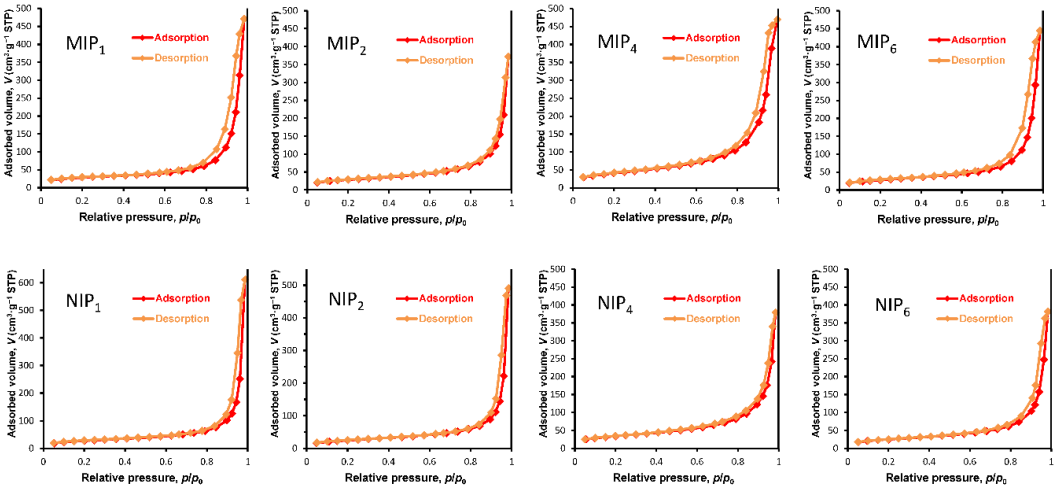

Figure S6. Adsorption and desorption isotherms collected by BET experiments.

Table S2. Specific surface area ($m^2 \cdot g^{-1}$) of MIP and NIP samples.

Samples	MIP_1 and NIP_1	MIP_2 and NIP_2	MIP_4 and NIP_4	MIP_6 and NIP_6
MIPs	101.4	103.9	151.8	102.0
NIPs	104.4	94.2	125.0	93.8

S.4. Adsorption as a function of temperature

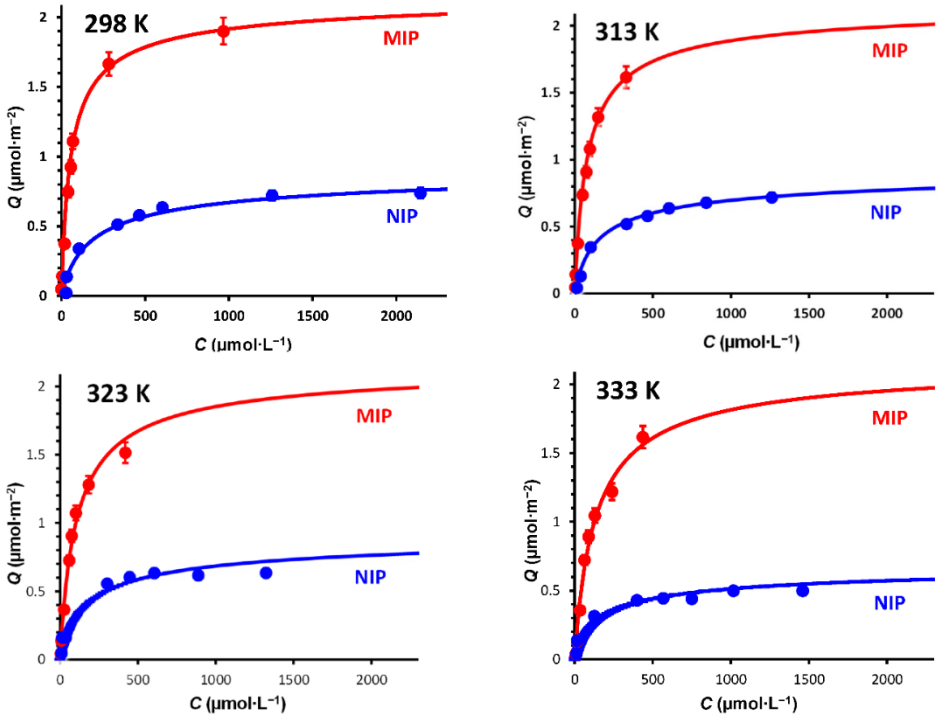

Figure S7. Adsorption isotherms of HA to MIP_4 and NIP_4 at different temperatures.

Table S3. Thermodynamic parameters of adsorption of HA to MIP_4 and NIP_4 at different temperatures.

Temperature		$Q_{max,s}$ (μmol·m^{-2})	K_s	$\Delta_{ads}G^0$ (kJ·mol^{-1})	$Q_{max,ns}$ (μmol·m^{-2})	K_{ns}	$\Delta_{ads}G^0$ (kJ·mol^{-1})
298 K	MIP	1.40	25000	−25.1	1.00	5000	−21.1
	NIP				1.20	4500	−20.8
313 K	MIP	1.40	16000	−25.2	1.00	5000	−22.2
	NIP				1.20	5500	−22.4
323 K	MIP	1.40	11000	−25.0	1.00	5000	−22.9
	NIP				1.20	5000	−22.9
333 K	MIP	1.40	8000	−24.9	1.00	5000	−23.6
	NIP				0.90	25000	−23.6

S.5. Calibration curves for the HPLC-MS analysis of histamine

Two stock solutions of HA (100 mg·L^{-1} and 300 mg·L^{-1}) were prepared in deionized water and stored at 4 °C. Working standard solutions were prepared by diluting the stock solutions to the ranges 0.5–10 ppm and 15–300 ppm for the determination of two calibration curves. All solutions were filtered through a 0.2 μm Nylon syringe filter before being analyzed by HPLC-MS [6,7]. The HA peak appeared 2.049 min after the injection of the HA solutions (Fig. S8). The HA calibration curves showed excellent linearity with $R^2 > 0.999$ (Fig. S9).

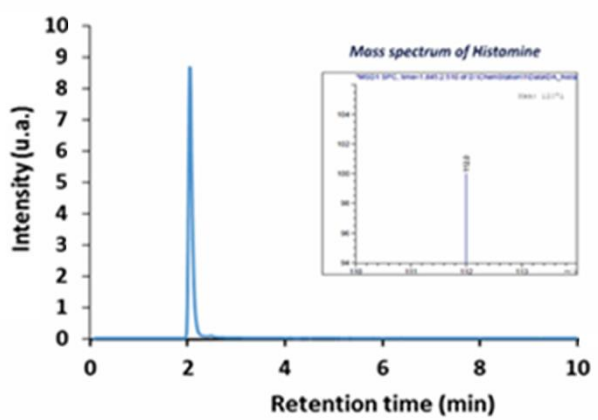

Figure S8. Chromatogram of histamine.

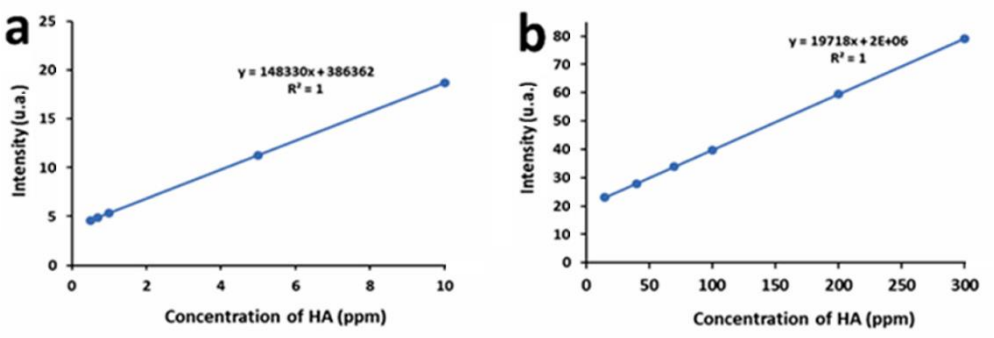

Figure S9. Calibration curves for histamine from 0.5–10 ppm (a) and 15–300 ppm (b).

S.6. Calibration curves of melamine and tyramine, and their analyses

Two stock solutions of MEL and TYR (100 mg·L^{-1}) were prepared in deionized water and stored at 4 °C. Working standard solutions were prepared by diluting the stock solutions to the ranges 0.5–5 ppm for the measurement of the calibration curves. All solutions were filtered through a 0.2 µm Nylon syringe filter before being analyzed by HPLC-MS. The MEL peak (Fig. S10a) appeared 2.334 min after the injection, and the TYR peak (Fig. S10b) appeared 4.238 min after the injection. The MEL (Fig. S11a) and TYR (Fig. S11b) calibration curves showed excellent linearity with $R^2 > 0.999$.

Chromatograms of residual HA, MEL and TYR in solution in analysis of adsorption to MIP_4 and NIP_4 by the depletion method are superimposed for showing the satisfactory resolution of the HPLC separation (Fig. S12).

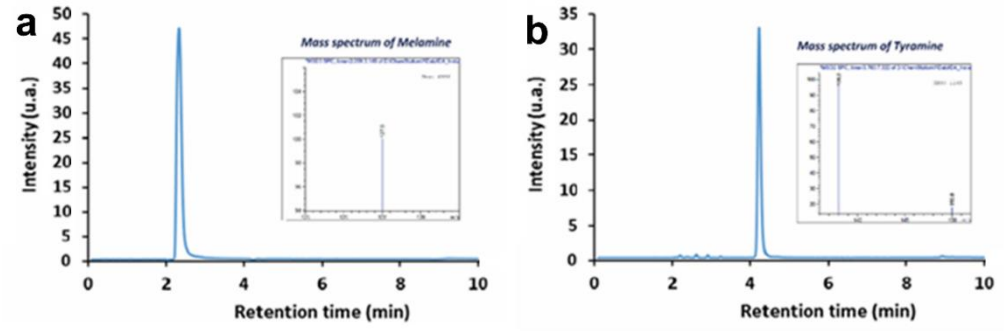

Figure S10. Chromatogram of melamine (a) and tyramine (b).

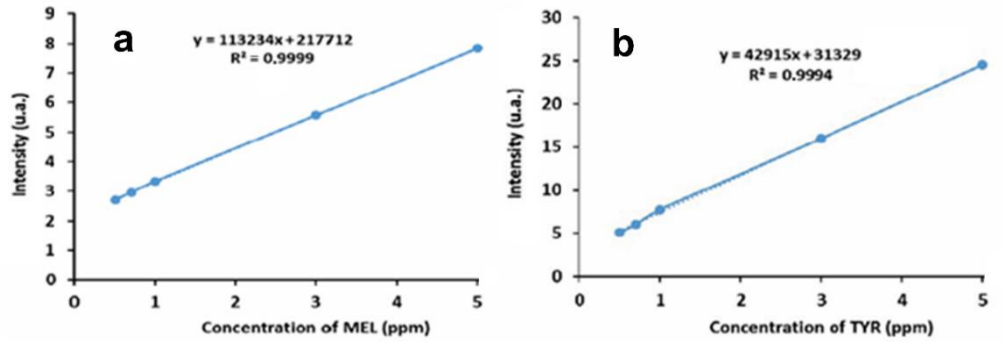

Figure S11. Calibration curve for melamine (a) and tyramine (b) from 0.5 to 5 ppm.

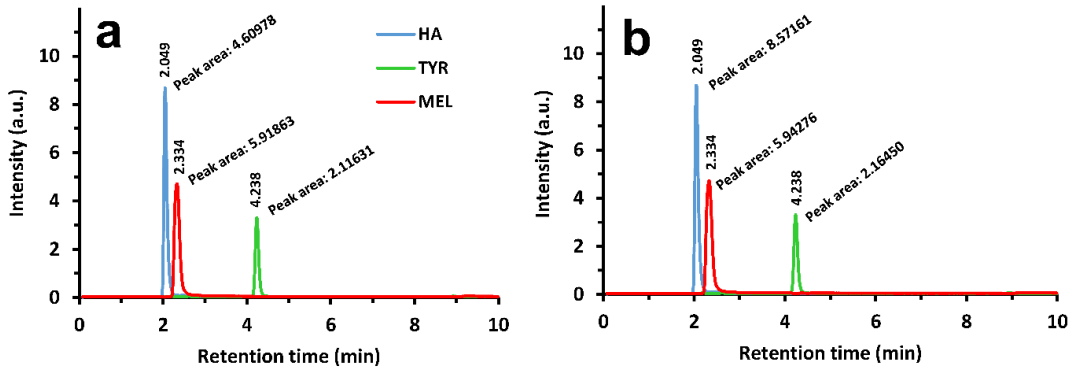

Figure S12. Chromatograms of HA (blue), MEL (red) and TYR (green) for analysis of adsorption to MIP_4 (a) and NIP_4 (b).

References

[1] G. Socrates, *Infrared and Raman Characteristic Group Frequencies - Tables and Charts*, 3rd ed, Wiley, Chichester (2001).

[2] I.A. Rahman, M. Jafarzadeh, C.S. Sipaut, Synthesis of organo-functionalized nanosilica via a co-condensation modification using γ-aminopropyltriethoxysilane (APTES), *Ceram. Int.* 35 (2009) 1883–1888, doi:10.1016/j.ceramint.2008.10.028.

[3] F. Pardal, V. Lapinte, J.-J. Robin, Modification of silica nanoparticles by grafting of copolymers containing organosilane and fluorine moities, *J. Polym. Sci. Part A Polym. Chem.* 47 (2009) 4617–4628, doi:10.1002/pola.23513.

[4] A. Anene, R. Kalfat, Y. Chevalier, S. Hbaieb, Design of molecularly imprinted polymeric materials: The crucial choice of functional monomers, Chem. Africa 3 (2020) 769–781, doi:10.1007/s42250-020-00180-1.

[5] M. Thommes, K. Kaneko, A.V. Neimark, J.P. Olivier, F. Rodriguez-Reinoso, J. Rouquerol, K.S.W. Sing, Physisorption of gases, with special reference to the evaluation of surface area and pore size distribution (IUPAC Technical Report). Pure Appl. Chem. 87 (2015) 1051–1069, doi:10.1515/pac-2014-1117.

[6] M. Dimitrijevic, S. Stefanovic, N. Karabasil, D. Vasilev, N. Cobanovic, N. Ilic, V. Djordjevic, UPLC-MS/MS determination of histamine levels in canned fish collected from Belgrade retail markets, *Meat Technol. (Belgr.)* 57 (2016) 47–56.

[7] C. Molins-Legua, P. Campins-Falcó, Solid phase extraction of amines, *Anal. Chim. Acta* 546 (2005) 206–220, doi:10.1016/j.aca.2005.05.021.